

D
EWR
~~1536~~
1536

Radon Emission Studies and Hydrogeochemical
Investigations of Tattapani Hot springs (Kotli, Azad
Kashmir, Pakistan)



By

Muhammad Anees

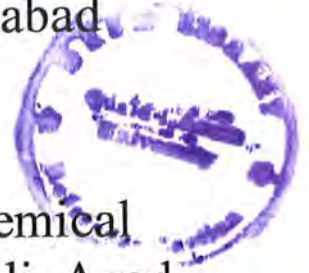
M.Phil. Geology

Department of Earth Sciences
Quaid-i-Azam University
Islamabad Pakistan

2013-2015



Department of Earth Sciences,
Quaid-i-Azam University, Islamabad



PEAR
1536

Radon Emission Studies and Hydrogeochemical
Investigations of Tattapani Hot springs (Kotli, Azad
Kashmir, Pakistan)

A Report Presented to

Department of Earth Sciences
Quaid-i-Azam University, Islamabad

In partial fulfillment
of requirement for the degree of

Master of Philosophy in Geology

By

Muhammad Anees

(02111313004)

2013-2015

CERTIFICATE

It is certified that **Muhammad Anees** has carried out all the work related to this Thesis report under my supervision at the Department of Earth Sciences, Quaid-i-Azam University, Islamabad and the work fulfills the requirement for award of M.Phil. degree in Geology.

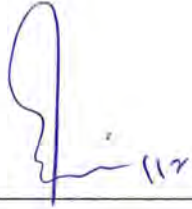
Research Supervisor: _____ 

Dr. Mumtaz Muhammad Shah

Assistant Professor,

Department of Earth Sciences,

Quaid-i-Azam University, Islamabad.



Chairman: _____

Prof. Dr. Muhammad Gulraiz Akhter

Professor,

Department of Earth Sciences,

Quaid-i-Azam University, Islamabad.



ACKNOWLEDGEMENTS

First of all I am humbly grateful to **Almighty Allah** for His help and guidance. I would also like to thank my supervisor **Dr. Mumtaz Muhammad Shah**, Assistant Professor, Department of Earth Sciences without whom, this dissertation would never have been completed.

I would like to show my heartfelt gratitude towards **Mr. Aziz Ahmad Qureshi** and **Dr. Shahid Manzoor** of the Physics department COMSATS Islamabad. Their help was pivotal in not only providing the necessary laboratory facilities for my thesis work, but also helping me in answering every query I had related to the realm of Physics. My most sincere acknowledgments to **Mr. Rafique Sheikh** of PINSTECH, Islamabad, without whose wise advices, I would have never been able to produce this document.

I am thankful to **Mr. Usman**, lab attendant at Radiation Physics Lab, COMSATS Islamabad, without whom, the RAD-7 data could never have been made possible. I am thankful to my parents and teachers for believing in me and standing by me in the difficult times in my life. Heartfelt gratitude to **Mr. Emadullah Khan** and **Mr. Tahir Hussain** for their help in sample collection at the Hot springs in Kotli.



Muhammad Anees

(02111313004)

ABSTRACT

Radon Emission Studies and Hydrogeochemical Investigations of Tattapani Hot springs (Kotli, Azad Kashmir, Pakistan)

Surface manifestation of geothermal water occurs in Tattapani town near Kotli district, Azad Kashmir, Pakistan. An integrated study focusing on radon emissions from soil gas and hydro-geochemistry of hot springs has been carried out for characterizing the subsurface geothermal system. This methodological combination of radon with hydrochemistry plays an important role in identifying the geothermal system and geologic controls on permeable zones, fluid origin and the overall flow pattern. Hot springs emerge from the carbonates of Muzaffarabad Formation (Cambrian) present in the core of Tattapani anticline with Paleocene to Eocene shales and limestone on its flanks. A part of intrusion exposed on NW limb of anticline along Cambrian-Paleocene rocks contact, has been considered to be an indication of subsurface heat source. Radon sampling was carried out over 36 sampling points with 200 m spacing in a 1 km² grid around the hot springs. Spatial distribution of radon concentration over the grid when overlapped with the surface geology, showed an anomalous zone over the Cambrian-Paleocene contact. Hydro-geochemistry data show that sodium-bicarbonate water the composition of hot spring water. The surface temperature of these springs is up to 60.8°C. Average reservoir temperatures based on silica and cation geothermometers are 110°C and 140°C respectively. A non-equilibrium state of fluid-rock as shown with Giggenbach ternary diagram (Na-K-Mg) suggests that a dissolution process in a low temperature condition is dominant. Data from oxygen and deuterium isotopes implies that thermal water is of meteoric origin and the source of recharge is probably rains and snow melts in the north at higher altitudes. Residence time based on tritium contents in thermal water is more than 60 years suggesting that they were recharged before thermonuclear testing in 1952. A conceptual model reveals that Tattapani hot springs are not associated with active magmatism. Instead a deep intrusion might generate the heat source for the hot spring waters that are recharged by predominately meteoric water. Fluid pathways are controlled by fractures in Cambrian carbonates. Overall, Tattapani hot springs, being immature and considered as low enthalpy system, are suitable for domestic purposes only.



TABLE OF CONTENTS

CHAPTER 1: INTRODUCTION

1.1	Introduction	1
1.2	Geothermal Resources of Pakistan	2
1.2.1	Geo-pressurized Geothermal Sources	2
1.2.2	Seismo-Tectonic and Suture Related Systems	3
1.2.3	Geothermal Systems related to Neogene-Quaternary volcanism	3
1.3	Study Area	5
1.3.1	Site and Accessibility	5
1.3.2	Previous Work	5
1.4	Aims and objectives	6
1.5	Methodology	6
1.5.1	Literature Review	6
1.5.2	Field Methodology	8
1.5.3	Lab Methodology	8

CHAPTER 2: REGIONAL GEOLOGY AND TECTONICS

2.1	Regional Tectonic Settings	9
2.2	Structural Settings of the Kotli area	11
2.3	Lithostratigraphy of Study area	12
2.3.1	Dogra Slate (Precambrian)	12
2.3.2	Muzaffarabad Formation (Cambrian)	13
2.3.3	Bauxite and Fire-clays (early Paleozoic to Early Cenozoic Eras)	13
2.3.4	Patala Formation (Paleocene)	15
2.3.5	Margala Hill Limestone (Eocene)	15
2.3.6	Chor Gali Formation (Eocene)	15
2.3.7	Basic Intrusions (Post-Eocene)	16

2.3.8	Murree Formation (Miocene)	16
2.3.9	Siwalik Group (Late Miocene to Pleistocene).....	17

CHAPTER 3: METHODOLOGY

3.1	Radon Measurements	18
3.1.1	RAD-7 Radon Detector	21
3.1.2	Radon Sampling	21
3.1.2.1	Grid Preparation	21
3.1.2.2	Soil-Gas Radon Measurement.....	23
3.1.2.3	Radon Measurement in Water.....	25
3.2	Hydrogeochemical Analysis.....	26
3.2.1	Sample Collection and Preservation.....	26
3.2.2	Physio-Chemical Measurements	26
3.2.3	Flow Rate Estimation	26
3.2.4	Major Ions Analysis	27
3.2.5	Stable Isotope Analysis	27
3.2.5.1	Stable oxygen isotope ($\delta^{18}\text{O}$) analysis of water samples.....	27
3.2.5.2	Stable hydrogen isotope ($\delta^2\text{H}$) analysis.....	28
3.2.5	Tritium Analysis.....	28

CHAPTER 4: RESULTS AND DISCUSSIONS

4.1	Field Observations.....	29
4.2	Soil Gas Radon Emissions.....	31
4.3	Physical Characteristics of Thermal Water	34
4.4	Chemical Composition of Hot springs	34
4.5	Geothermometry.....	38
4.5.1	Silica Geothermometry.....	38
4.5.2	Cation Geothermometry	39
4.6	Origin of Thermal Waters	41

4.7	Residence Time	43
4.8	Conceptual Model	44
CHAPTER 5: CONCLUSIONS AND RECOMMENDATIONS		
5.1	Conclusions	46
5.2	Recommendations	47
REFERENCES		48
APPENDIX-I.....		56
APPENDIX-II		62

LIST OF FIGURES

Figure 1.1: Map showing occurrences of geothermal systems in Pakistan	4
Figure 2.1: Regional Tectonic map of North Pakistan.....	10
Figure 2.2: Geological Map of Kotli area.	14
Figure 3.1: Radon emanation process in a geothermal field.....	19
Figure 3.2: Isotopes of Radon with their decay chains	20
Figure 3.3: Google Earth (top view) contemplation of sampling grid.....	22
Figure 3.4: Soil-gas radon measurement diagram.	24
Figure 3.5: Diagram for radon measurement in water	24
Figure 4.1: Geological map of study area showing radon sampling points.....	30
Figure 4.2: Contour map showing spatial distribution of radon	33
Figure 4.3: Behaviour of radon over traverse across anticline	33
Figure 4.4: Ternary plot showing type of geothermal water	35
Figure 4.5: Piper plot based on major ions showing chemical nature of water	35
Figure 4.6: Schoeller plot showing trends in concentration of ions.....	36
Figure 4.7: Bar chart showing calculated reservoir temperatures.....	40
Figure 4.8: Na-K-Mg ternary plot showing maturity of thermal water	40
Figure 4.9: Plot between isotopes of hydrogen and oxygen	42
Figure 4.10: Conceptual model of Tattpani geothermal system	45

LIST OF TABLES

Table 1: Radon concentration at sample locations around hot springs.....	56
Table 2: Physical characteristics of water samples.....	57
Table 3: Concentration of major ions along and radon in water samples.....	58
Table 4: Calculated reservoir temperatures using silica geothermometers.....	59
Table 5: Reservoir temperatures calculated using cation geothermometers.....	60
Table 6: Results of isotopes analysis; tritium, deuterium and oxygen.....	61

CHAPTER 1

INTRODUCTION

1.1 Introduction

Pakistan has been an energy deficient country for the over a decade with frequent power shutdowns in summer season. Hydroelectric stations on rivers and thermal power plants (consuming fossil fuel) are main sources of power generation with some contribution from nuclear power plants. Residents of under developed and remote areas are most affected by this power shortage. Despite having enormous potential energy resources, Pakistan remains an energy deficient country, which is evident from the fact that most of its inhabitants still lack the luxury of uninterrupted supply of electricity. There are numerous hot springs in Pakistan having varying degrees of temperature (including boiling water) with substantial discharge rates. These geothermal fields need to be studied for their assessment as potential sources for power generation. High potential sources could be exploited to generate electricity while low potential sources can be used for domestic purposes like space heating and green houses to grow vegetables particularly in winters.

The geotectonic framework of Pakistan supports the idea of presence of exploitable sources of geothermal energy. Presence of various geothermal indicators like alteration zones and fumaroles in many regions of Pakistan, numerous hot springs in different parts of the country, and Quaternary volcanism (Shuja, 1986) promises a bright prospect for geothermal energy in Pakistan. Geothermal activity in Pakistan originates due to the collision between Indian and Eurasian Plates which resulted in creating the regional tectonic imprints like Main Karakoram Thrust (MKT) and Main Mantle Thrust (Bakht, 2000). Another geothermal zone extending from NW to SE of the country, occurs as a narrow axial belt along the Indus basin margin all the way down to Karachi. Chagai volcanic arc, formed as a result of neotectonic volcanism due to the subduction of the Arabian Plate beneath the Eurasian Plate (Zaigham et al., 2009).

Surface manifestations as hot springs provide an excellent evidence of a sub-surface potential geothermal energy source that could be evaluated and exploited as an energy source. Geochemical analysis of water from hot springs could provide a fair assessment about chemical nature and temperature of its heat source, which could help to identify its

potential use. Radon measurements help in identifying possible pathways (faults and fractures) for tracing the fluid movement. This study has been carried out for radon measurements and to investigate geochemical properties of Tattapani hot springs located near Kotli, Azad Kashmir, Pakistan.

1.2 Geothermal Resources of Pakistan

Pakistan is located at the junction of Indian and Eurasian plates forming an active seismic belt through Pakistan. This seismic belt is an indication of a broad geological past comprising of significant geotectonic events, e.g., which contain:

- Rifting between Iran–Afghanistan microplates resulting Panjal traps in Kashmir (Permian-Carboniferous volcanism).
- Rifting of the Indo-Pakistan (Indian) Plate (Upper Jurassic to Lower Cretaceous).
- Emergence of a “hot spot” in the region responsible for extensive volcanism creating Deccan traps (Upper Cretaceous).
- Development of a series of volcanic landmasses (Kohistan and Ladakh Island arcs) along the northwestern margins of Indian Plate.
- Collision of between Indian and Eurasian Plates followed by uplifting of Himalayas (Cretaceous–Paleocene).
- Subduction of Arabian Plate under Eurasian Plate causing volcanism in Chagai area (Neogene–Quaternary).

Surface manifestations of geothermal energy in Pakistan found within geotectonic zones can be categorized in three geothermal environments, i.e., the seismo-tectonic or suture-related systems, the geo-pressurized systems related to basin subsidence, and the systems related to Neogene–Quaternary volcanism (Figure 1.1).

1.2.1 Geo-pressurized Geothermal Sources

In geo-pressurized systems, the normal heat flow is trapped by insulating impermeable beds in a rapidly subsiding sedimentary basin. It is an account of their great depth (as much as 6,000 m) that temperatures ranging from less than 93°C to more than 150°C are encountered. They commonly contain pressurized hot connate water at pressures ranging from 40 % to 90 % in excess of the hydrostatic pressure corresponding to the depth.

Gradual subsidence has led to the ultimate isolation of trapped pockets of water contained in alternating pervious and impervious sequences. In Pakistan, such geo-pressurized zones exist within the Lower Indus basin in southern Sindh province along the western margin of the Indus Plain and in the Potwar Basin of Punjab province (Figure 1.1). The available information indicates the association of the geothermal zones with south-Sulaiman, south-Kirthar, and Lower Indus geological structures. In Karachi, two hot springs exist one at ManghoPir and one at Karsaz. The geological setting of the south-Kirthar geothermal zone is similar to that of the south-Sulaiman geothermal zone.

1.2.2 Seismo-Tectonic and Suture Related Systems

Geothermal regimes in the north of Pakistan, as manifested by many thermal springs, are associated with sutures related structures. Karakorum, Hindukush and Himalayan thrust and fold belts, showing very strong seismic activities are most prominent geomorphological features of this region. The hot spring sites of Chitral region are associated with the Hindukush fault system. In Gilgit-Hunza region the hot springs of Murtazabad, Budelas, Sassi and Dassu are associated with Main Karakorum Thrust (MKT), whereas the hot springs of TattaPani, Sassi, and Mushkin are associated with the Main Mantle Thrust (MMT) (Shuja and Sheikh, 1983; Todaka et al., 1999). Surface manifestations in the form of hot springs are also scattered in the Indus and Balochistan sedimentary basins, which are mainly associated with seismotectonic and suture zones. Hot springs are present in many parts of Balochistan, associated with faults, which show significant seismic activity (Bakr, 1965; Kazmi, 1979; Quittmeyer et al., 1979).

1.2.3 Geothermal Systems related to Neogene-Quaternary volcanism

Geothermal systems associated with the Chagai Magmatic Arc are manifested by mineralized thermal springs, which are largely confined to the Koh-e-Sultan volcano and appear in the vicinity of the Miri crater (Fig.1). This region apparently has the highest geothermal potential in Pakistan and an economically exploitable geothermal reservoir may be expected in the southwestern part of Koh-e-Sultan.(Shuja and Khan, 1984). The aeromagnetic investigations, done in a large area of Chagai Volcanic Arc and the Kharan Trough, have revealed a number of buried volcanic plugs, necks and stocks all over the Chagai region, which could be very important targets for the exploitation of geothermal energy.

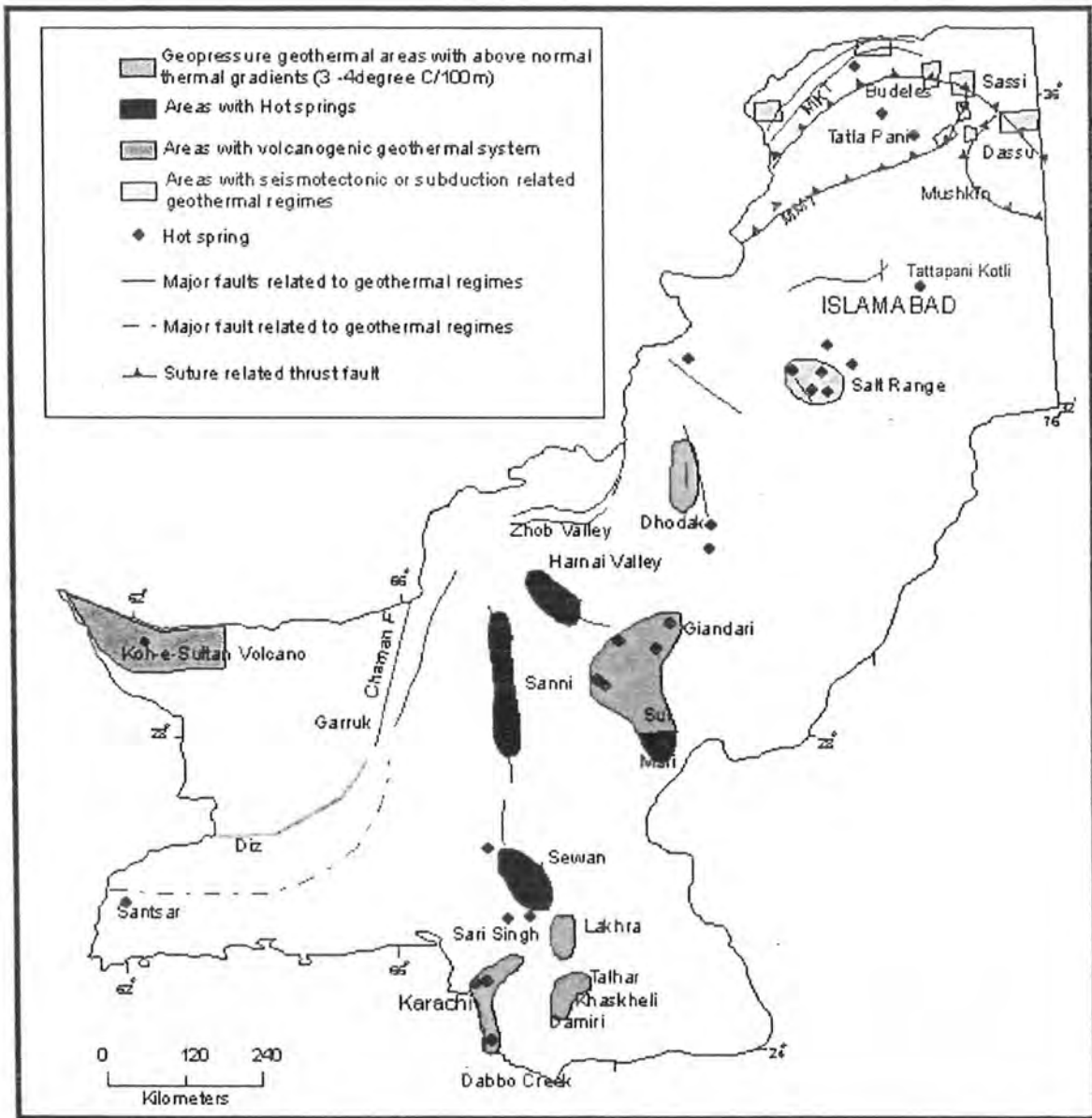


Figure 1.1 Map showing the geothermal manifestations in Pakistan (source: GSP- Geological Survey of Pakistan). Study area is depicted in this map near Islamabad.

1.3 Study Area

1.3.1 Site and Accessibility

Tattapani town located 26 km north of Kotli city which is at three hour drive, at a distance of 150 km towards East of Islamabad. The survey has been carried out for the measurement of radon emissions and fluid geochemistry in and around the Tattapani Hot springs, Kotli which is located in Azad Kashmir, North Pakistan. The study area is located at 34°36'47" N Latitude and 73°56'49" E Longitude. Tattapani Hot springs emerge in gravelly bank of Ponch River and discharge directly the river. Surface manifestations occur as numerous springs from a major site on north bank of river, having variable flow rates. The samples for hydro-geochemical analysis were easily collected on site but ground radon measurements were made in 1 km² grid around the main hot spring site where most of sampling points were located on high relief terrain and were collected with an error of ± 25m.

1.3.2 Previous Work

The earlier geologists in late 1800s started working on stratigraphy and tectonics of Kotli area. Verchere (1867) and Lydker (1883) studied regional geology and stratigraphy of this area and initially used the term of "Nummulitic Limestone" for Paleogene rocks. Later studies were focused on organic rich rocks of Kashmir called "Subathu" of Eocene age along with Miocene Murree and Miocene-Pleistocene Siwalik Group (Wadia, 1928). A detailed paleo-environmental study on Paleogene sequence of Kotli area in Azad Kashmir was initially carried out by Wells and Gingerich (1987). Lithostratigraphy of Kotli area range in age from Precambrian to Recent consisting mainly of sedimentary rocks with minor intrusions of basic sills and dykes (Ashraf et al., 1983). Kotli area has also been successfully explored for coal deposits ranking Bituminous to anthracitic coal occurring in the Paleocene rocks (Ashraf et al., 1986). Munir and Baig, 2006 provided an ample input in the novel direction related to the biostratigraphy of the Paleogene sequence of Neo-Tethys Sea exposed in Tattapani area, Kotli.

1.4 Aims and objectives

The aims and objectives of this study are:

- To delineate the zones of anomalous radon emanation with reference to hot springs and subsurface heat source.
- To develop and correlate a radon distribution map with the subsurface geology of the area.
- To find out chemical nature and subsurface reservoir temperature using major ion study of spring water.
- To calculate residence time and origin of thermal water using isotopes study.
- To develop a conceptual model of geothermal systems on basis of acquired results and correlate it with the geology of the region.

1.5 Methodology

1.5.1 Literature Review

Radon survey is an inexpensive, accurate and a quite easy technique to monitor geothermal activity and detect the occurrence of permeable zones in a geothermal field. This technique measures the radioactivity of radon as a parameter to determine the characteristics of study area. Radon measurement technique was initially applied in mineral exploration, mainly for delineating subsurface uranium ore bodies. Radon (^{222}Rn) is produced as a gas in decay chain of Uranium (^{238}U). Radon is an effective indicator of the hidden uranium deposits and its usage have been widely understood and pragmatic. Application of radon as tool in the exploration of geothermal resources was derived from mineral exploration techniques. Active fault zones have anomalous radon concentrations because they offer a pathway for its accumulation and upward migration (Ioannides et al., 2003; Jönsson, 1995; Swakon et al., 2004). Radon measurement technique is typically used as a geochemical device (Geochemistry tools). Cox in 1980 used solid-state radon detectors in Hawaii for geothermal exploration. Application of radon for geothermal

exploration began to popularize in 1984 (Gingrich, 1984). Radon investigation for delineating geothermal zones has been useful in New Zealand and USA (Whitehead, 1984; Fleischer, 1988). Radon as a tool in geothermal exploration has been used in Mexico by Lopez et al., 1987 and Balcazar et al., 1993 to delineate the subsurface origin of geothermal energy, and later it applied to monitor geothermal activity in Las Pailas geothermal area, Costa Rica (Rodriguez et al., 2008). Radon method can detect hidden faults quite easily and effectively (Fu et al., 2005). Karingithi and Wambugu (2010) stated that the radon measurement was carried out in Arus and Bogoria geothermal regions to detect permeable zones. Moreover, a qualitative study of activity of radon in some of the geothermal areas in Mexico was done by Balcázar et al., in 2011. Previously, radon method has been successfully implemented for petroleum exploration e.g. China, Mongolia and England (Zuhui et al., 1993; Duddrige, 1994). Radon survey for exploration of geothermal areas in Indonesia has been carried out in Ungaran and Rajabasa geothermal fields by Phuong et al., 2012 and Haerudin et al., 2013 respectively.

Unfortunately, research related to hydro-geochemistry geothermal sources in Pakistan is still in early phase. Reconnaissance studies on geothermal areas of Pakistan has been carried out in terms of geological settings and common hydrochemical investigations (Todaka et al., 1988). Detailed studies focusing on hydrogeochemical properties and geothermal parameters such as nature and evolution of geothermal water (chemical origin, age, rock-fluid interaction and calculation of subsurface reservoir temperatures) have been carried out on hot springs of Northern areas of Pakistan (Ahmad et al., 2000; 2001; 2002). Recently, hydro-geochemical investigations have also been carried out on hot springs in areas like Chagai and Potwar (Ahmad et al., 2005; 2008; 2009). Knowledge of various geothermal parameters like the origin, physicochemical nature, mixing processes, residence time and subsurface reservoir temperature are crucial to prospection of a geothermal system. These geothermal parameters can be calculated by incorporating environmental isotopes analysis along with hydrogeochemical methods. Most frequently used environmental isotopes are; ^{18}O , ^2H and ^3H of water, ^{13}C and ^{14}C of dissolved inorganic carbon (DIC), ^{18}O and ^{34}S of sulphates. Applications of isotopic and geochemical methods for geothermal studies were contemplated by Truesdell et al., (1977); Krouse (1980); Giggenbach (1982) and Giggenbach et al. (1983).

1.5.2 Field Methodology

RAD7, an electronic detector was used to measure radon concentration in ground (soil) and water samples. Radon in ground (soil) was measured on spot using a stainless steel probe supplied by Durrige Company (USA). Radon concentration was measured by recoding a resultant alpha activity through the circulation of air in loop for a period of 20 minutes. Water samples were analyzed in field for radon concentration after collection from the hot springs, cold spring, river and open well in the field. The RAD H₂O technique of RAD7 was used to calculate concentration of radon levels in water. This technique takes approximately 30 minutes to completely analyze radon concentration in water samples. Physico-chemical parameters like electrical conductivity (EC), temperature, total dissolved solids (TDS), pH, and flow rate were measured in the field. For chemical and isotopes analysis water samples were collected in plastic bottles with air tight caps to avoid alteration in fluid chemistry.

1.5.3 Lab Methodology

Chemical analyses were carried out using: atomic absorption spectrophotometry for Na, K, Ca and Mg; UV-visible spectrophotometry for SiO₂; titrimetry for SO₄, HCO₃ and Cl (APHA, 2005). The ⁶¹⁸O value of the water was measured by mass spectrometer using the CO₂ equilibration technique (Epstein and Mayeda, 1953). ⁶¹⁸O values of water were analyzed relative to V-SMOW with a standard error of ±0.1‰. The tritium content of the samples was calculated using liquid scintillation counting after electrolytic enrichment of the water samples with a standard error of ±1 TU (Hussain and Asghar, 1982).

CHAPTER 2

REGIONAL GEOLOGY AND TECTONICS

2.1 Regional Tectonic Settings

Himalayas were originated as a result of the collision between Indian and Eurasian Plates about 50 Ma ago (Johnson et al., 1976). 130 Ma ago, Indian plate separated from the Gondwanaland and started drifting northward. This northward drift of Indian plate started closure of the Neo-Tethys; located between the Indian and Eurasian plates (Norton and Sclater, 1979). An intra-oceanic subduction developed Kandahar, Nuristan and Kohistan-Ladakh arcs simultaneously with closure of Neo-Tethys (Treloar and Izzat, 1993; Searle et al., 1999). For almost 40 million years, this arc-related magmatism continued (Pettersson and Windley, 1985). The Kohistan-Ladakh arc collided with the Eurasian plate to its north, closing the back-arc basin in between them and it developed an Andean type continental margin. Main Karakorum Thrust (MKT), marks the tectonic boundary, created as a result of this collision of Kohistan-Ladakh arc with the Eurasian plate (Malinconico, 1989). Neo-Tethys continued its subduction underneath the Kohistan-Ladakh arc till the leading edge of the Indian plate had been completely consumed and finally the collision of Indian plate with the remnant of Kohistan-Ladakh arc (Powell, 1979). This collision has been proposed at about 65~50 Ma and as a result of this episode, the Main Mantle Thrust (MMT) was formed (Maluski and Matte, 1984; Treloar et al., 1989; Tonarini et al., 1993; Rowley, 1996).

Four regional fault systems; Main Karakorum Thrust (MKT), Main Mantle Thrust (MMT), Main Boundary Thrust (MBT) and Himalayan Frontal Thrust (HFT), divide Pakistani Himalayas into five major tectonic domains. (Yeats and Lawrence, 1982). DiPietro and Pogue (2004) named these tectonic domains as: Karakorum Block, Kohistan Island Arc, Northern Deformed Fold and Thrust Belt, Southern Deformed Fold and Thrust Belt and Punjab Foredeep.

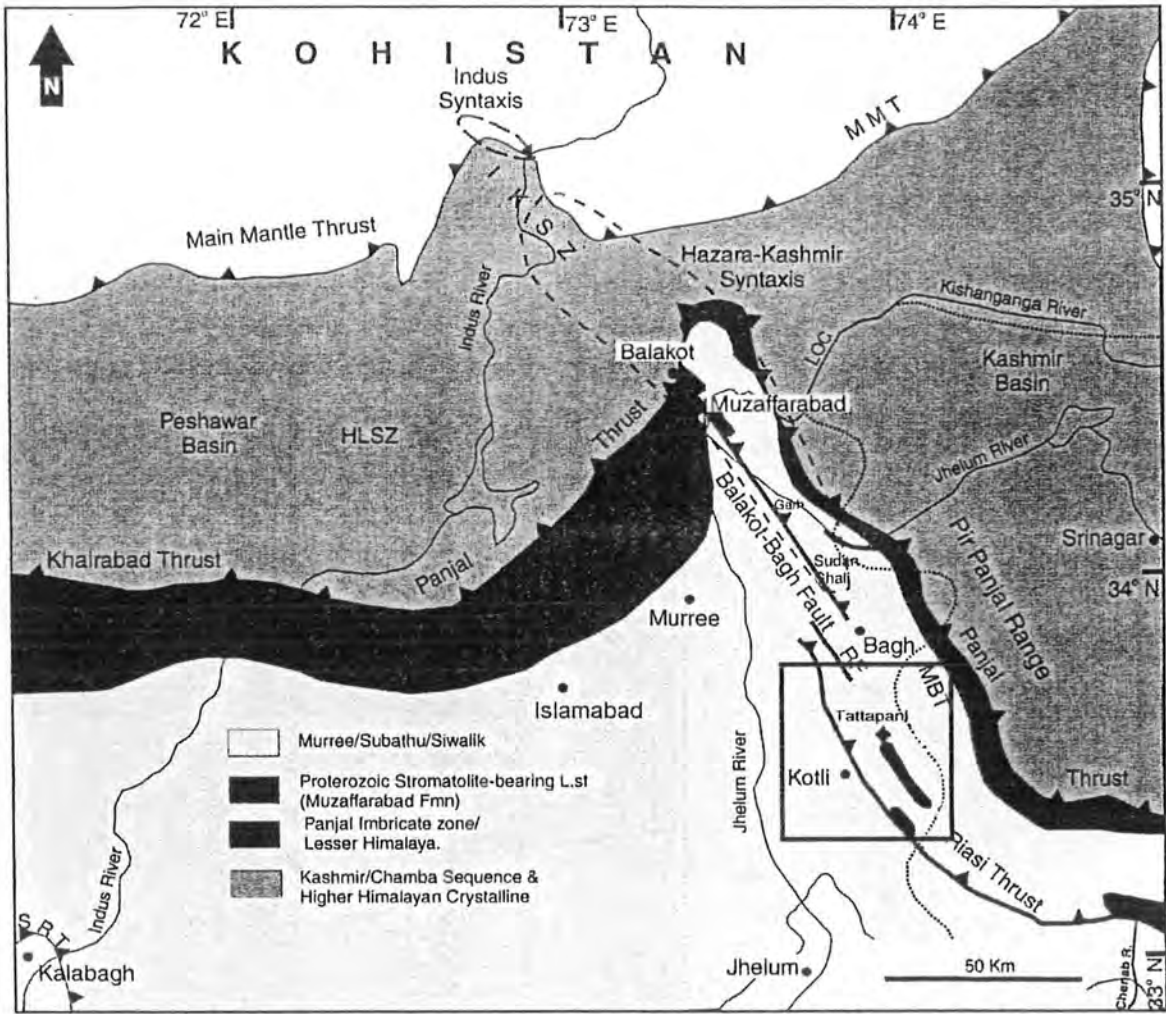


Figure 2.1 Regional Tectonic Map of NE Pakistan (modified after Thakur et al., 2010) showing major thrusts formed due to collision of Indian and Eurasian Plates. Box shows proximal tectonic settings of study area (Tattapani). Riasi thrust in the south, MBT (Main Boundary Thrust) in northeast and Balakot-Bagh Fault in northwest.

Generally, Himalayas are subdivided into Higher Himalayas; bounded between MMT and MCT (North to South), Lesser Himalayas with the MCT to its north and MBT to the south and to further south of this MBT there is the Sub-Himalayas with non-marine clastic strata dominated by the Murree Formation and overlying Siwalik Group, with the active Himalayan Front thrust at the base. Indus–Tsangpo suture zone containing ophiolites and ultramafic rocks truncates on the north into High Himalayan sequence, marking the original boundary of the India–Eurasia collision.

The Main Boundary Thrust (MBT) takes a sharp bend from northwest to south forming Hazara–Kashmir Syntaxis (HKS). On the western limb of this syntaxis, Muzaffarabad Formation extends in a northwest-southeast trend towards Balakot from Muzaffarabad. This unit is overlain by the Paleocene Patala Formation and by the non-marine succession of Murree Formation to the northeast (Wadia, 1931). While southwestern contact of this unit of Muzaffarabad Formation is faulted against the Miocene rocks. The Muzaffarabad anticline (Fig. 2.1), with a fault running at its Southwest margin, brings Pre-Cambrian Muzaffarabad limestone against the Siwaliks in a juxtaposition with each other. This fault is named as the Balakot–Bagh fault in literature (Yeats et al., 2006; Hussain et al., 2009). The mapped surface rupture shows 3–7 m vertical separation and three segments of coseismic faulting which are collectively called the Balakot–Bagh Fault (Kaneda et al., 2008). To the southeast of this BBF, two en-echelon anticlines have exposed Muzaffarabad Formation near Kotli (Hussain et al., 2009). The Muzaffarabad Formation here, is overlain by Patala Formation and Murree Formation, showing a similar geological setting as that of Muzaffarabad anticline. Southwest margin of the southwestern anticline of the Muzaffarabad Formation is demarcated by a set of NW-SE trending faults, named as the Riasi Thrust (Fig. 2.1). Wadia (1937) demarcated the Main Boundary Thrust (MBT) in Kotli area, separating the units of limestone, nummulitics and Murrees in the hanging wall from the footwall containing Siwaliks. Rawalakot fault is described as an intervening between the Riasi Thrust and the BBF (Hussain et al. 2009).

2.2 Structural Settings of the Kotli area

The Kotli area lies to the southeast of the Hazara-Kashmir syntaxis in sub to lower Himalayas. Plunging anticlines represent the prominent structural features of this region. The "Main boundary fault" of Wadia (1928) passes through the center of this area in a

NW-SE direction. Major folds in the area also follow the general NW-SE axial trend, showing a noticeable parallelism with fold axes of Pir Punjal Range (Wadia 1928). Palana-Divigarhand Tattapani-Karela anticlines are two huge plunging anticlines striking as the major structural features of the area.

The Tattapani-Karela anticline trending NW-SE with a 15° to 30° plunge is over 28 kilometers in length and 4.5 kilometer in width with Tattapani to its north and Karela to the south. Muzaffarabad formation is exposed in the core of this anticline while Paleogene and Miocene formations on its flanks. NW-SE trending Palana-Devigarh anticline, 11 km in length and 3 km in width, plunging between 15° to 25° , has a faulted contact between Murree and Muzaffarabad Formations at its south-western limb. Patala Formation is exposed all along the fault plane in discontinuous patches. The syncline between these two anticlines is names as Barmoch Syncline with its axis trending in the same NW-SE direction as that of the anticlines. The younger Murree formation comprises the core of the syncline, whereas the older Eocene limestone, Patala Formation, Bauxite and Muzaffarabad Formations are present on the flanks.

The Main Boundary Fault (Riasi thrust) trending NW-SE, passes from the southeast of the area, where the Murree Formation has been placed against the Siwalik Group along this fault. Near the village of Bangang, an offshoot fault (the Bangang fault) truncates the SW limb of Palana-Devigarh anticline (Aadil and Rehman, 2013).

2.3 Lithostratigraphy of Study area

The lithostratigraphic units in the area mainly consist of sedimentary rocks ranging from Precambrian to Recent with minor igneous bodies. A brief detail of exposed lithostratigraphy of the Kotli and Tattapani area is as follows;

2.3.1 Dogra Slate (Precambrian)

The Precambrian 30-45 meters thick slates forming steep slopes and escarpments are exposed at Nail Nala on 43 K/3 toposheet according to the Geological of Survey of Pakistan. The slates are dark gray to black in color, exhibit well-developed slaty cleavage. Lithology of this stratigraphic unit is defined to be argillaceous, thinly bedded and fine-

grained slates, with lenticular quartz veins along joints and cleavage planes. 2-8cm grains of pyrite are reported in the lower part of the unit. A 1-1.5 meters thick brecciated bed overlies these slates in study area (Kotli).

2.3.2 Muzaffarabad Formation (Cambrian)

Muzaffarabad Formation can be observed in the core of anticlines in this area. It is composed of two members mainly; a lower member composed of dolomite and an upper quartzite member. It has been observed during this study as well as reported in literature (Ashraf et al., 1983), that the base of the Muzaffarabad Formation is not exposed in Kotli area. The dolomite member can be divided into three different zones. The basal zone is thin to thick bedded, fine grained, light grey to cream in color, having numerous cherty layers and bands. The middle zone consists of dolomite, which is thin-bedded and of grey to dark grey color. The uppermost zone is also composed of dolomite, which is light grey, having chert bands in the topmost horizons with thickness ranging from a few mm to 50 mm. In Palana-Bangang and Goi areas, quartzite member overlies the cherty dolomite. It is well developed and is exposed at the south-eastern plunge of Khuiratta anticline from Devigarh peak to Bangang. The upper quartzite member is made up of fine-grained, snow-white to white quartzite, having brownish to yellowish layers of weathered surfaces exposed along the joints. The thickness of quartzite is measured to be from 9 meters to 21 meters. Upper zone is frequently brecciated at the top and is overlain unconformably by bauxitic clays and bauxite.

2.3.3 Bauxite and Fire-clays (Early Paleozoic to early Cenozoic Eras)

The bauxite and fire-clays unconformably lie over the Muzaffarabad Formation in this area, with brecciated dolomites, abundant quartz pebbles at the contact. Three zones can be distinguished within this unit on the basis of lithological variation and physical characteristics. These zones are: brecciated zone, non-pisolitic bauxite and pisolitic bauxite zone. Brecciated zone is at the base, and is composed of aluminous to calcareous clays, with abundant quartz and chert pebbles. This zone is 1.5 to 3 meters thick. Lower zone consists of non-pisolitic bauxite or fireclay and its composition is cream to grey and sometimes dark grey clays. There is a sharp contact between fire-clays and the underlying brecciated zone. The contact between the upper pisolitic bauxite is transitional.

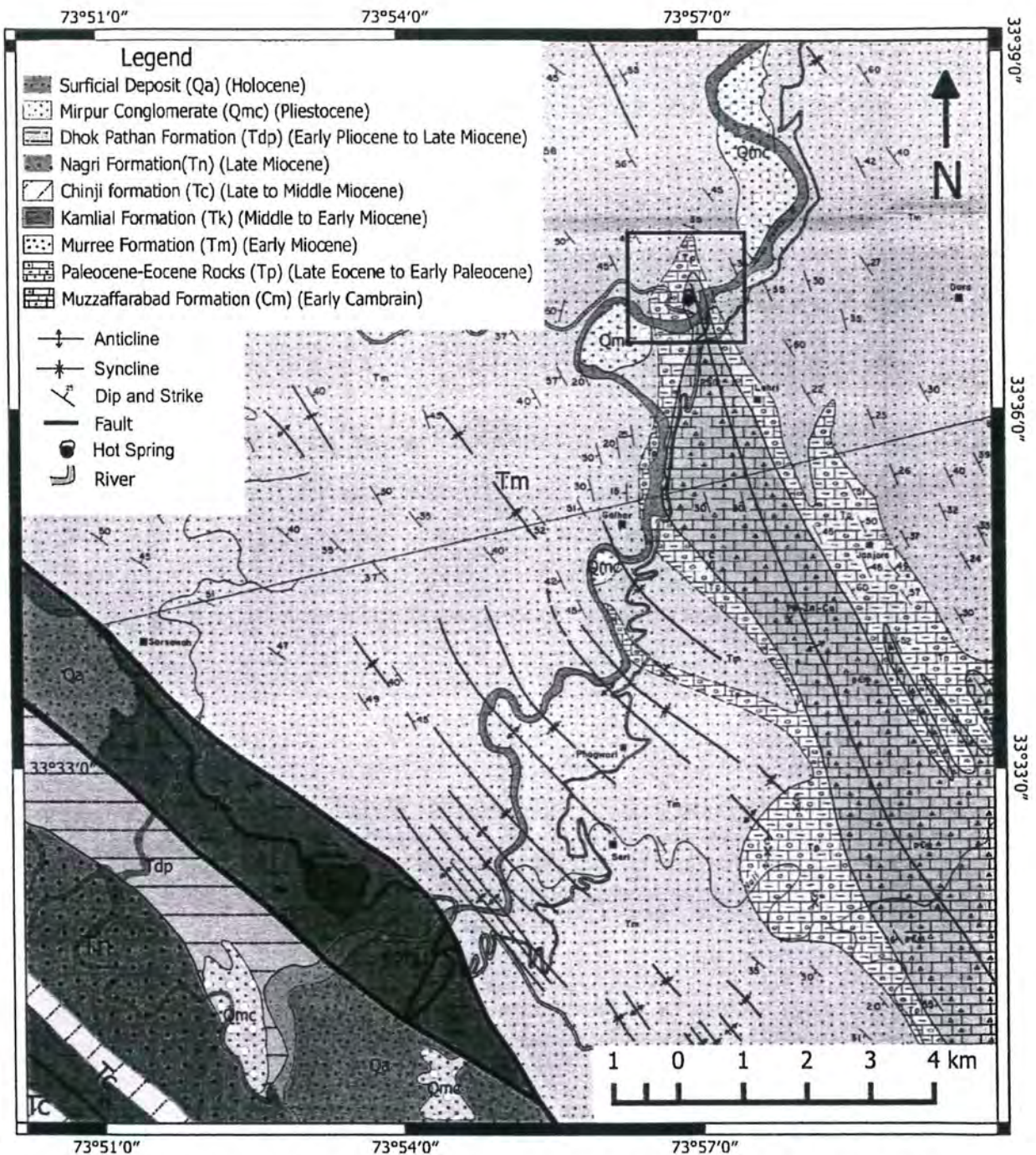


Figure 2.2 Geological Map of Kotli area (modified after GSP G43/14) showing Tattapani anticline as a major structural feature. Study area is indicated by a box on the northern most part of Tattapani anticline.

2.3.4 Patala Formation (Paleocene)

In the Kotli area, bauxite and fire-clays are overlain by Patala Formation. However, at places, Muzaffarabad Formation directly underlies the Patala Formation. The absence of bauxite-fire-clays may be interpreted as result of their erosion prior to the deposition of Patala Formation. The Formation is up to 43 meters and is composed of silty to splintery dark grey to black shales with minor interbedded limestone. Lenticular coal seams are found at two horizons within these shales (Ashraf et al., 1986). The basal part is near contact of Patala Formation with bauxite-fire-clays, while the upper part is roughly 12 m above the lower part. The beds are compacted and hard being phosphatic, having phosphatic nodules of dark grey to black color. The Patala Formation forms a transitional contact with overlying Margala Hill Limestone. The Lockhart Limestone is not present in this area at its chronostratigraphic position; between Hangu and Patala Formations (Munir and Baig, 2006).

2.3.5 Margala Hill Limestone (Eocene)

Margala Hill Limestone overlies Patala Formation with a transitional contact. The Formation is separated from Patala Formation on the basis of faunal variation and higher proportion of limestone to shale. Lithologically it is composed of fine to medium grained, medium to thick-bedded, grey, dark grey to black limestone with subordinate greenish grey shales. The limestone is quite similar to that in Patala Formation, while the shales are silty and splintery in nature. The nodularity is well-developed in limestone with individual nodules varying from 6 to 15 cm across. Nodules of pyrite are quite common on fresh surfaces, which is due to effects of weathering have left cavities on bed surfaces. Milky calcite veins and calcite patches are frequently present within the limestone. Well-developed nodules of limestone have been found embedded in silty shales at Nikial and Tattapani.

2.3.6 Chor Gali Formation (Eocene)

The Chor Gali Formation is composed of limestone, marly limestone, argillaceous limestone, marl and subordinate shale. The limestone shows a flaggy/platy appearance. The flaggy habit is probably due to the increasing marl intercalations. The limestone

weathers to creamy light yellow and light grey colors. The freshly broken surfaces are light grey. The Margala Hill Limestone transitionally grades into the Chor Gali Formation (Munir and Baig, 2006). Alternating beds of hard and platy limestone within the shale sequence are characteristic features of Chor Gali Formation.

2.3.7 Basic Intrusions (Post-Eocene)

Igneous intrusive bodies; mainly mafic sills and dykes are present in many parts of Kotli area. Although, these intrusions are mainly associated with dolomite of Muzaffarabad Formation, they are also seen to be penetrating the overlying bauxite/fire-clay and Paleocene/Eocene rocks at certain places. Wadia (1928) has also reported such basic bodies to have intruded the Eocene rocks and thus are supposed to be post-Eocene in age. The altered dolerite intrusion known as Samelote Intrusion, is the largest known intrusion in this area. It is more than 300 m long and up to 90 m wide. The basic body has penetrated the dolomite, fire-clay and bauxite. The contacts of the basic body with the country rocks are not clear due to scree and alluvium. The intrusive rock is medium to coarse grained with fresh surfaces having dark bluish grey to greenish-grey color. Color of weathered surfaces is light grey. At Guni Maini, an intrusion of about 30 x 9 m is found to be intruding the country rock (dolomite). A small marble deposit is present at the contact possibly formed due to thermal effects of intrusion on dolomite (Ashraf et al., 1983).

2.3.8 Murree Formation (Miocene)

The Murree Formation is composed of alternating series of shales and sandstones of mainly buff color, however, grey, green and purple colored facies are also quite common. Murree Formation is divided into a lower and an upper part, on lithological basis (Wadia, 1928), which can be recognized in field. Generally, lower part of the Formation is composed of hard, fine-grained, ferruginous, non-micaceous, deep -red, purple to grey the sandstone with frequent pseudo conglomerate beds at various horizons. The associated shales are red, purple and splintery, but occasionally greenish grey shales are also present at the base of the formation. Calcite patches are abundant and rare limestone nodules can also be seen. Presence of structural features like tight isoclinal and over folds with repeated faulting and fractures indicate a compressional regime.

Upper Murree Formation consist of pale grey to brownish grey, soft, coarse grained micaceous sandstone with red, purple, buff and grey shales interbeds. Murree Formation have its characteristic red/purple color due to the oxidation of iron minerals. Upper part of Murree Formation shows open, broad folds which have been weathered into strike ridges and valleys with a succession of escarpments and dip slopes (Ashraf et al., 1983).

2.3.9 Siwalik Group (Late Miocene to Pleistocene)

The Siwaliks can be sub-divided into four distinctive formations: Soan Formation (Pleistocene), Dhok Pathan Formation (Pliocene), Nagri Formation (Upper Miocene) and Chinji Formation (Middle Miocene). Soan Formation makes up the upper part of the Siwalik Group. It is composed of conglomerates, very poorly sorted sandstones with siltstones and shales. Dhok Pathan Formation consists of mainly red and brown colored clays, with some gray colored shale units at some places representing a cyclic deposition of clays and sandstones. The upper part of this Formation also contains radioactive horizons. Nagri Formation follows Dhok Pathan Formation downwards by the massive sandstones with very few volcanoclastic shale hatches (Nagri Formation). Chinji Formation marks the base of Siwalik group with maroon colored shales along with subordinate sandstones.

CHAPTER 3

METHODOLOGY

3.1 Radon Measurements

Radon is a distinctive element which is produced as a radioactive gas in the decay chain of uranium and can be mechanically transported in soil through diffusion and convection (Tanner, 1964). Radon in high concentration has been measured over faults, geothermal zones, uranium deposits and volcanoes (Nishimura and Katsura, 1990). It is an excellent natural radioactive tracer of hydrothermal reservoirs in geothermal energy prospecting, because convection transport phenomena is a dominant radon migration process, due to the high pressure and temperature gradients in the geothermal field, resulting in high radon concentrations at the surface of geothermal field. Radon is transported together with other gases as CO₂, H₂, N₂ and CH₄ by advection mechanism in the upward direction (Balcazar et al., 2014), due to the enormous pressure gradient produced by the thermodynamic activity of the geothermal reservoir as deep as 1 km to 3 km. The hydrothermal activity generates gases that transport radon to the earth surface faster than the diffusion process and transported to the surface easily through open faults and fractures. Radon being a noble gas it does not form compounds and there is no need for geochemistry corrections (Balcazar et al., 2011).

Radon (²²²Rn) is a decay product of Radium (²²⁶Ra); both belong to the natural radioactive chain of Uranium (²³⁸U). Radon has three isotopes, ²¹⁹Rn (Actinon), ²²⁰Rn (Thoron) and ²²²Rn (Radon); ²¹⁹Rn does not produce any interferences in the detection system for two reasons: firstly it comes from ²³⁵U whose abundance in soil and rocks is 1/137 of that of ²³⁸U; and secondly ²¹⁹Rn has half-life of only 4 seconds which means that in about 24 seconds (six half-lives) its concentration is reduced to about 3%. As far as ²²⁰Rn is concerned, it comes from the decay series of ²³²Th, whose abundance can overcome that of ²³⁸U in ratios ²³²Th/²³⁸U as big as 8.2 for quartz monzonite and granite; the corresponding ²²⁰Rn half-life is 56 seconds, therefore any detection system has to suppress ²²⁰Rn contribution from that of ²²²Rn. Two kinds of detectors can be used for determining radon concentration in the field: plastic detectors and ionization chamber (electronic detectors).

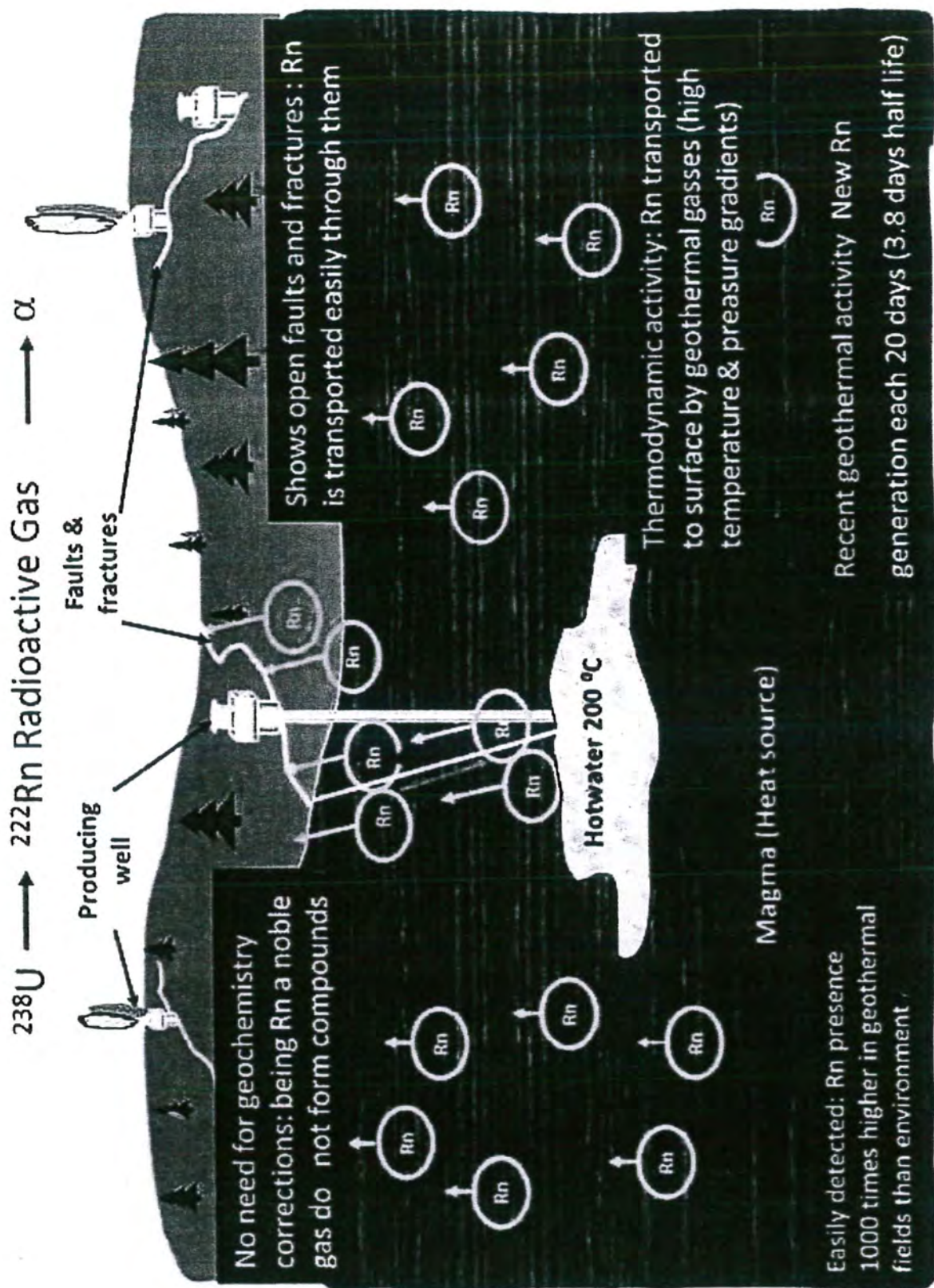


Figure 3.1 Radon emanations in a geothermal field (after Balcazar et al., 2014). Radon concentration is greater over faults and fractures.



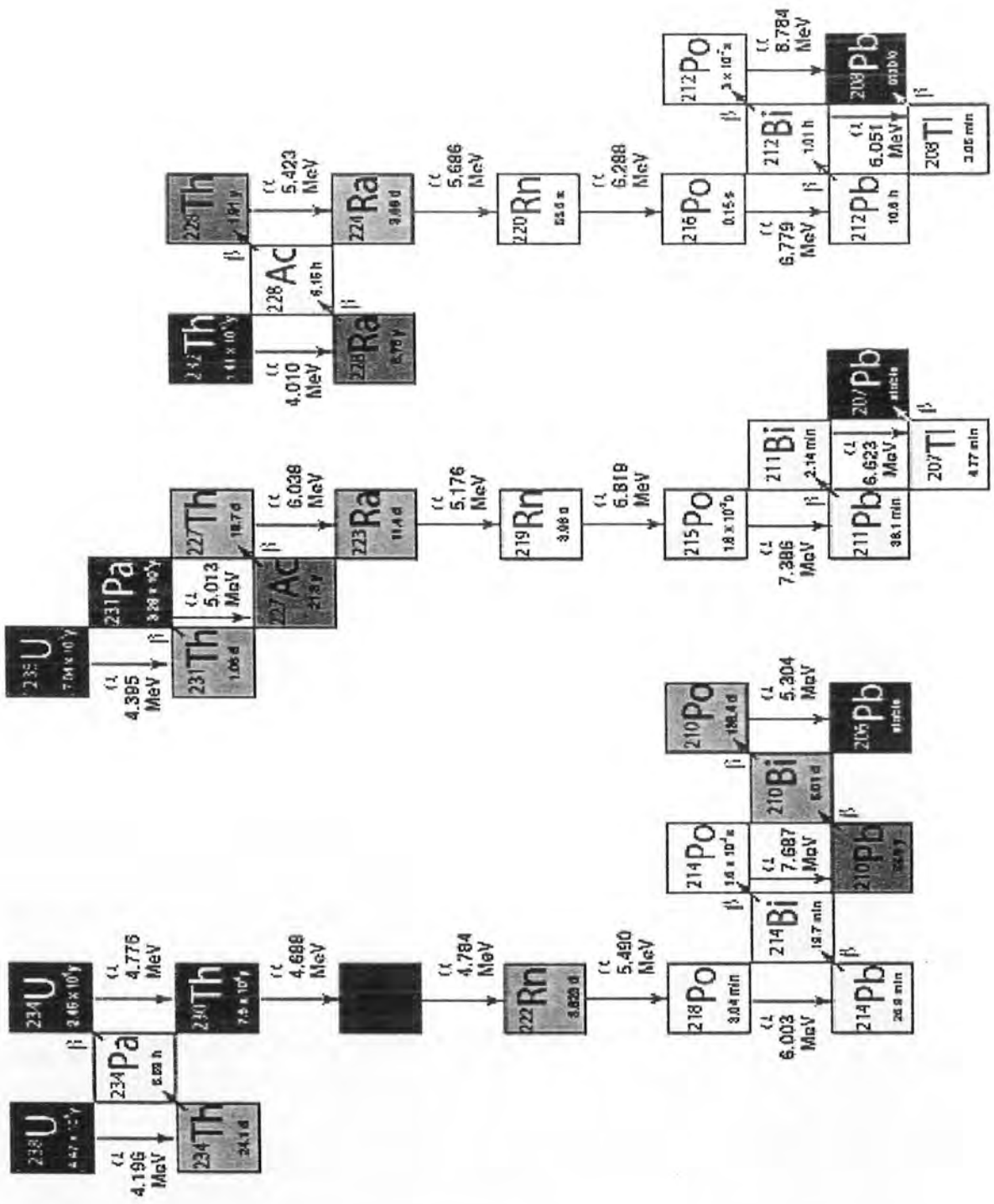


Figure 3.2 Decay chains of three isotopes of Radon. From left to right, ^{222}Rn (Radon) a product of ^{238}U decay, ^{219}Rn (Actinon) product of ^{235}U and ^{220}Rn (Thoron) a daughter of ^{232}Th .

3.1.1 RAD-7 Radon Detector

RAD7 Electronic Radon Detector (DURRIDGE Company Inc.) is used for measurement of radon at Tattapani area. This equipment contains an air pump which is connected to a solid state alpha detector containing a semiconductor (usually silicon) for conversion of alpha radiations into electrical signals. RAD-7 has the capability to instantly distinguish between radon and thoron by detecting the corresponding energy released by emitted alpha particle through a technique called alpha spectrometry. RAD7, in normal mode, has a sensitivity of 0.508 CPM/(pCi/L). Radon concentration can be represented in three units by RAD7, i.e. CPM (counts per minute), Bq m⁻³ and pCi l⁻¹. The units selected for present study were Bq m⁻³, while in case of high count rates kBq m⁻³ can also be used.

3.1.2 Radon Sampling

Sampling was based on a grid chart, designed over a region around Tattapani Hot springs, in such a way that it covered sufficient area around with respect to local geology and hot springs to generate an anomaly map. Sampling grid consisted of sampling locations fixed on perpendicular positions at equal spaces from each other. Purpose in opting this type of sampling, was based on, vegetation, outcrop morphology, topography and ease of accessibility. Grid sampling is usually carried out to cover large area for low cost and high time efficiency and can be an effective method to collect data with precision.

3.1.2.1 Grid Preparation

Grid was made over hot springs site, using Google Earth version 6.1. The grid was plotted so that it covered an area of 1 km². In total, 36 sampling points were contemplated in such a way that they fulfilled objectives and purpose of sampling. Each point signified a specific value of longitude and latitude over the map. The grid for sampling was designed and plotted by intersecting six N-S trending lines like 1 to 6 and six E-W trending lines labeled as A B C D E F. The distance between two neighboring N-S and E-W trending lines was 200m, so that proposed 36 sampling locations could be plotted. The intersection of these lines yielded sample labels like A1, B1, and C1 etc. as shown in Figure 3.3.

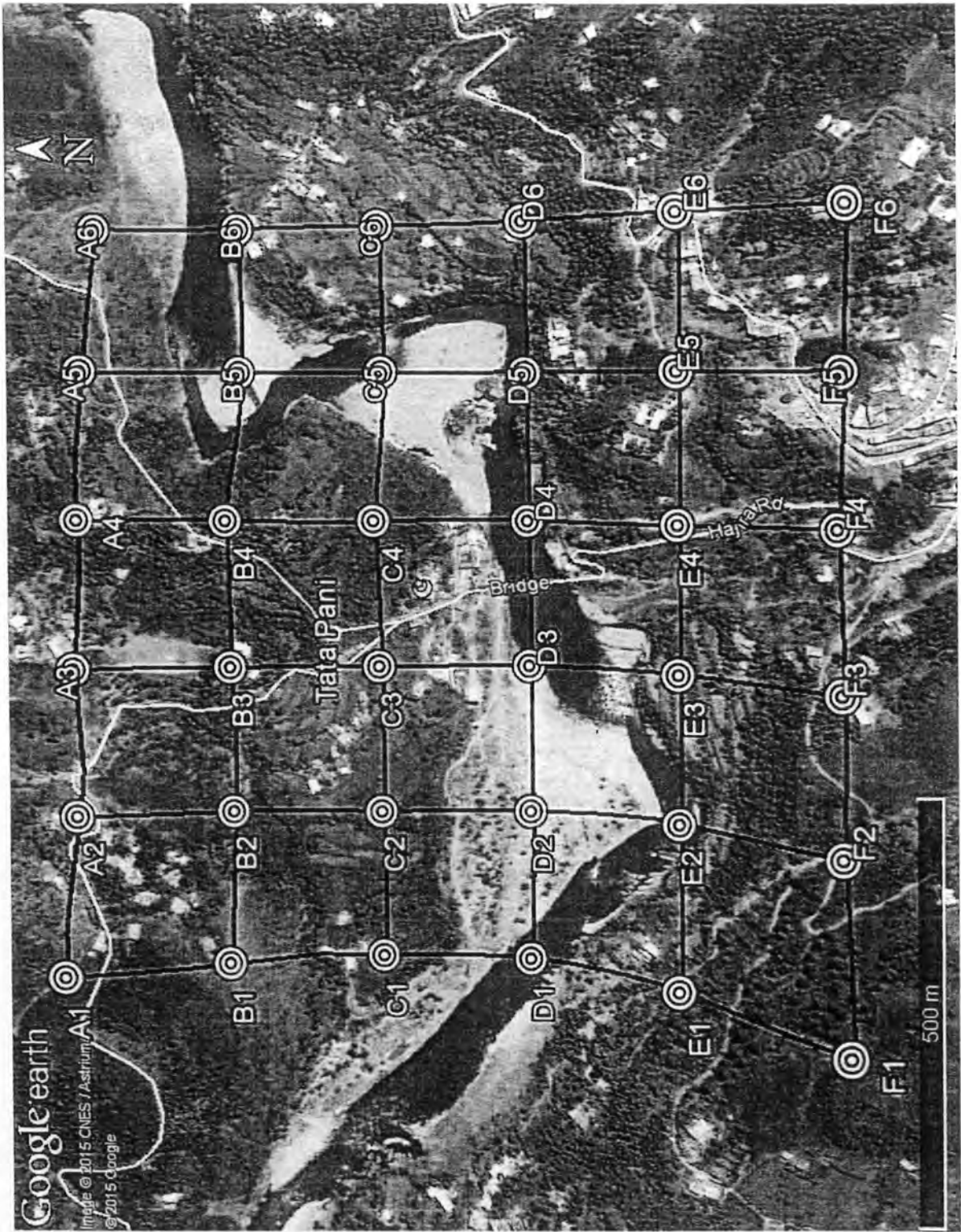


Figure 3.3 Google Earth (top view) contemplation of sampling grid plotted over Tattapani area.

Based on proposed grid, latitude and longitude were obtained using Google Earth. These coordinates corresponded to a particular sample location, for example; A1 was located at 33°37'0.58"N and 73°56'26.65"E. List of the entire sample coordinates is given in Table 1. Magellan GPS was used in order to locate a particular sample point corresponding to the specific coordinates. However, a few sampling locations were not feasible due to topographic and residential limitations. So some samples, encountered in these circumstances, were taken at ±40m from the proposed site of collection.

3.1.2.2 Soil-Gas Radon Measurement

Radon in soil-gas was measured with the help of RAD7 electronic detector. DurrIDGE Company (USA) provides stainless steel soil-gas probe along with RAD7 to extract and quantify radon levels in the soil. Probe was inserted in ground by hammering a 2 cm wide hollow tube 50 cm deep into the soil. In case of river bank and rocky areas where soil cover was enough to allow the steel shaft to reach at desired depth, hole was made using a steel rod to achieve maximum depth. Steel probe was connected to RAD7 through rubber tubes which were connected by hose connectors. A water trap was also connected where required in order to prevent entrance of water present in soil into the detector. Once RAD7 is turned on, it starts pumping air from the soil into the probe and then in the water trap. After that, the air is passed through a desiccant tube to remove any moisture, then to an air filter and finally to the RAD7 (Figure 3.4). Hole was properly sealed with the soil every time before the start of counting process in order to avoid mixing of gas with air from atmosphere. Air from the soil was pumped for 20 minutes into the RAD7 and allowed to circulate with in an open loop to record the resultant alpha activity. The time period in RAD7 to analyze concentration of radon over a single location is called a "run", and it takes 20 minutes (4 cycles) to complete of one run in a Sniff protocol mode to calculate radon concentration in Bq/m³. Values of recorded from all four cycles were averaged to get mean radon concentration at each point at that time.

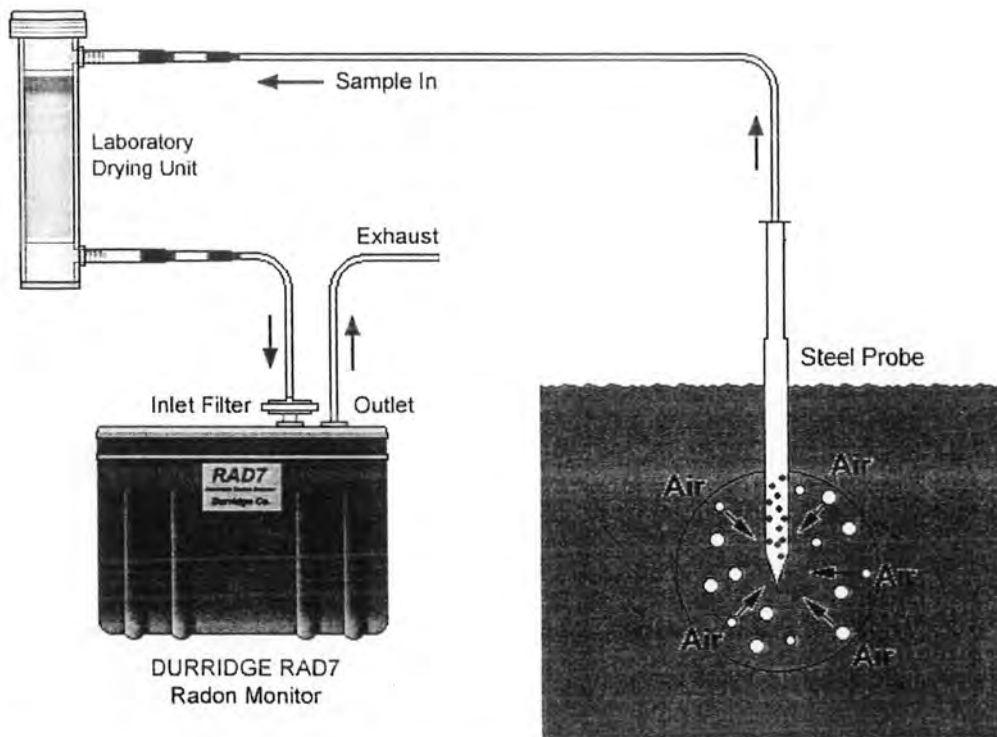
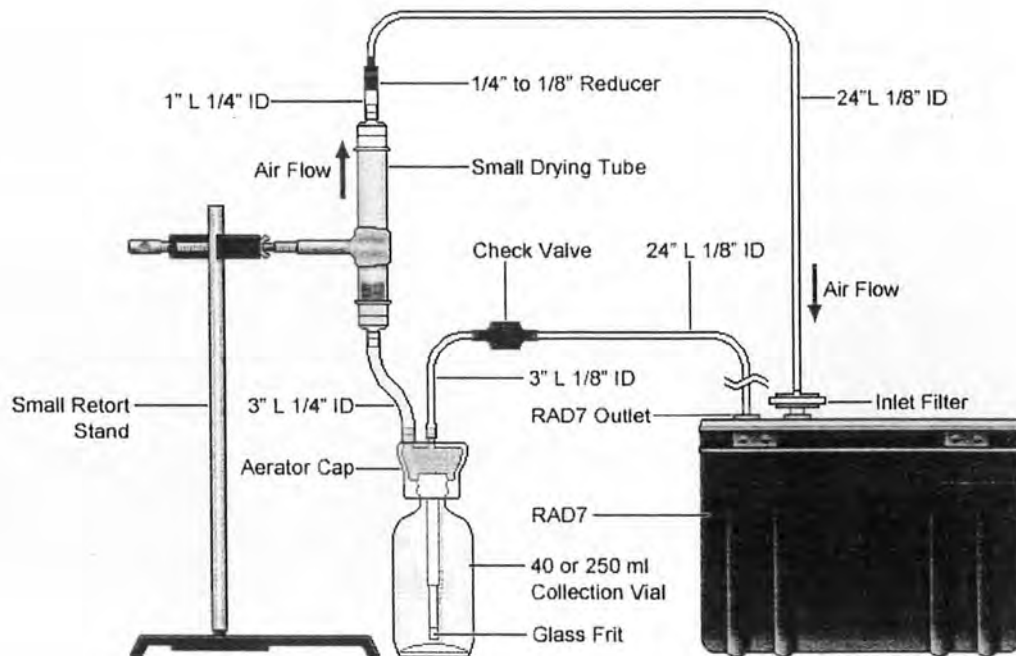


Figure 3.4 A simplified diagram displaying arrangement of apparatus for the radon measurement in soil.

RAD H₂O Configuration



© DURRIDGE Company, Inc.

Figure 3.5 Diagram showing arrangement of RAD H₂O apparatus for radon measurement in water samples using a 250 ml bottle.

3.1.2.3 Radon Measurement in Water

To analyze radon levels in water samples, RAD H₂O technique of RAD7 was applied which determined concentration of radon in water quite accurately. Water samples were analyzed in the field for determination radon levels after collection from hot springs, cold springs, river and tap water in the field. RAD H₂O technique uses specific and standard protocols to determine radon concentration in water samples. A time period of 30 minutes is required by RAD7 to completely analyze radon concentration in water. Two built-in preset configurations are provided in RAD7 according to the volume of vials (40 and 250 ml). A 250 ml vial is used in current study for the calculation of the radon concentration and was multiplied by the volume of the air loop. An aeration design in a closed circle is incorporated in this technique to keep the volume of water and air constant (Lee and Kim, 2006). RAD H₂O apparatus involves, RAD7, 250 ml water sample vial with aerator and a desiccant tube as shown in Figure 3.5. Air contact was minimized during the sample collection to avoid dilution of radon in samples. Wat 250, a preset protocol setting offered in RAD7 setup was used for measuring concentration of radon in water 250 ml vial. Radon is dissolved in water and to extract the dissolved radon from water samples during a close air loop experiment, the sample bottle was connected to the RAD7 and air was circulated in the loop using internal air pump of the RAD7. Air was re-circulated through the water constantly for 5 minutes so that equilibrium state would be achieved. The built-in pump of RAD7 initiates pumping automatically for 5 minutes at the start of experiment, thus aerating the sample which results in radon release from the sample and this radon is delivered to the RAD7 chamber for measurement. Most of the prevailing radon, approximately 94% is degassed from the water into the air loop during the first 5 minutes of aeration. The pump stops after aerating the sample for 5 minutes and then pauses for further 5 minutes. The counting is started subsequently. After every 5 minute cycle, a short report is printed by the system for the next 20 minutes. A printer attached to RAD7 prints a summary of experiment after 30 minutes showing the average concentration of radon in four measured cycles (each of 5 minutes), a bar chart of these analyses and a cumulative spectrum.

3.2 Hydrogeochemical Analysis

3.2.1 Sample Collection and Preservation

For chemical and isotopes analysis water samples were individually collected in high quality Polyethylene PET plastic bottles i.e., 200 ml each for cations, anions, silica, and isotopes (^2H , ^{18}O), while 1L for analysis of ^3H . Samples collected for cations analysis, were acidified with conc. HNO_3 to avoid precipitation upon storage. Samples collected for SiO_2 were diluted (1:1) with deionized water to prevent silica polymerization (Arnórsson, 2000). Samples were filtered in case of river water using filter paper (0.45 μm) while in case of samples from other location filtration was not required.

3.2.2 Physico-Chemical Measurements

Physico-chemical parameters such as water temperature, pH, flow rate, Total dissolved solid (TDS) and electrical conductivity (EC) were determined in the field. Temperature and pH measurements were made using Crison pH-meter PH25+. PH25+ was calibrated by using three buffer solutions of pH 4, pH 7 and pH 9, respectively. Electrode was placed into the water sample and left until thermal equilibrium is established. Readings were recorded up to 0.01 pH-units together with the temperature of the water. For Electrical conductivity and total dissolved solids, a multimeter was used. Electrode was washed with deionized water before and after the measurement to ensure the precision.

3.2.3 Flow Rate Estimation

Flow rates (estimate) were measured as the time taken for a float to travel a set distance in the outflow channel measured with a stop-watch and the cross-sectional area of the channel is determined. The flow rate is then estimated from:

$$\text{Flow rate (L/s)} = [(\text{channel length} \times \text{width} \times \text{depth}) \times 0.85] / \text{time}$$

Time is in seconds and that all dimensions are in decimeters (1dm = 10cm, and 1dm³ = 1L). As the surface velocity of a stream or outflow is faster than the mean velocity of the discharge a correction factor (0.85) was applied to the expression (Nicolson, 1993).

3.2.4 Major Ions Analysis

Chemical analyses were carried out using atomic absorption spectrophotometry using Varian Flame Atomic Absorption Spectrometer. A direct read out is given for concentrations of Na, K, Ca and Mg (Giggenbach and Goguel, 1988; AOAC, 2000) in mg/l. UV-visible spectrophotometry for was carried out SiO₂, which is analyzed as Si in water. For concentration of major anions in water samples like HCO₃, Cl and SO₄, titrimetry method is applied (APHA, 2005).

3.2.5 Stable Isotope Analysis

The stable isotope analyses were accomplished using Varian Mat GD-150 Mass Spectrometer. Stable isotope data is reported as Standard Mean Ocean Water (SMOW) for Oxygen (¹⁸O) and Hydrogen (²H) isotopes. The overall analytical errors were ± 0.1 ‰ for δ¹⁸O and ±1 ‰ for δ²H measurements. For isotope study, mass spectrometer vaporizes water samples and converts them gaseous phase (vapors). Since different sample preparation arrangements were applied for analysis of δ¹⁸O and δ²H, which were customized accordingly in laboratory. Each system is briefly detailed below.

3.2.5.1 Stable oxygen (δ¹⁸O) isotope analysis of water samples

For stable oxygen isotope analysis, an equilibrating system was used to equilibrate water samples with CO₂ gas. ¹⁸O/¹⁶O ratios from equilibrated CO₂ were then analyzed on mass spectrometer (Epstein and Mayeda, 1953). For simultaneous equilibrium of water samples, an equilibration system is equipped with reaction vessels which are made of glass with each vessel of 62 ml volume. These glass reaction vessels were attached to the manifold and vacuum line through grounded joints and capillaries respectively. To lower the free cross sectional area to about 0.2 mm², a stainless steel wire was inserted into the capillary. These vessels were immersed in a water bathtub for achieving homogeneous temperature of 22 ± 0.1°C. For initial degassing and equilibration of CO₂- H₂O system, vessels were coupled to a vibrator for shaking of samples. CO₂ of known isotopic composition was added into the reaction vessels after de-gassing of water samples. Magnetic switches were used for sealing the vessels and the vessels were vibrated to shake contents for suitable oxygen isotopic exchange. For equilibration, a time of 12-15 hours was provided and after that, measurements were made.

3.2.5.2 Stable hydrogen isotope ($\delta^2\text{H}$) analysis

For analysis of ^2H in water, water samples were reacted with Zinc shots. Zinc shots were prepared by first washing 5 g zinc shots with 200 ml of 1% nitric acid for one minute. After that, zinc shots washed 4-5 times with distilled water and acetone to remove any leftover acid. The zinc shots were then air dried and were placed in the glass vessel to dry under rotary vacuum pump. The glass container was gradually heated up to a temperature of 300°C in a furnace in order to degas zinc shots completely. After Heating, the glass vessel was cooled down to room temperature. 250 mg of Zn-shots were taken and added at the bottom Pyrex glass Kontess ampoule with Teflon stoppers. The ampoule was instantly locked and air was sucked out using rotary and diffusion pumps up to 1×10^{-3} Torr. $8\mu\text{L}$ of water having room temperature was added in ampoule in the presence of flowing argon gas. Ampoule is dipped in liquid nitrogen trap to freeze water and gases that remained non-condensed in the ampoule were pumped out. Ampoule was then heated at 480°C for 30 minutes. Subsequently, ampoule was allowed to cool down at room temperature. Hydrogen gas which was produced throughout heating process was analyzed for $\delta^2\text{H}$ isotopic composition. (Coleman et. al., 1982, Kendall and Coplen, 1985).

3.2.6 Tritium Analysis

Tritium in water samples was measured by counting beta decay counts using liquid Scintillation Counter (LSC). 10 ml simple aliquot was mixed with scintillation compound that discharges a photon when bombarded with beta particles. Photomultiplier tubes can counter transform the photons into electrical pulses that are calculated over a time period of many hours. Calibrated standards and blanks were used to compute and associate the counts obtained from results. Direct liquid scintillation counting has an accuracy of ± 7 to ± 110 TU. Electrolytic enrichment is often required before counting for hydrological studies in order to reduce uncertainty. The enrichment was achieved using cells with phosphated mild steel cathodes and stainless anodes (Florkowski, 1981).

CHAPTER 4

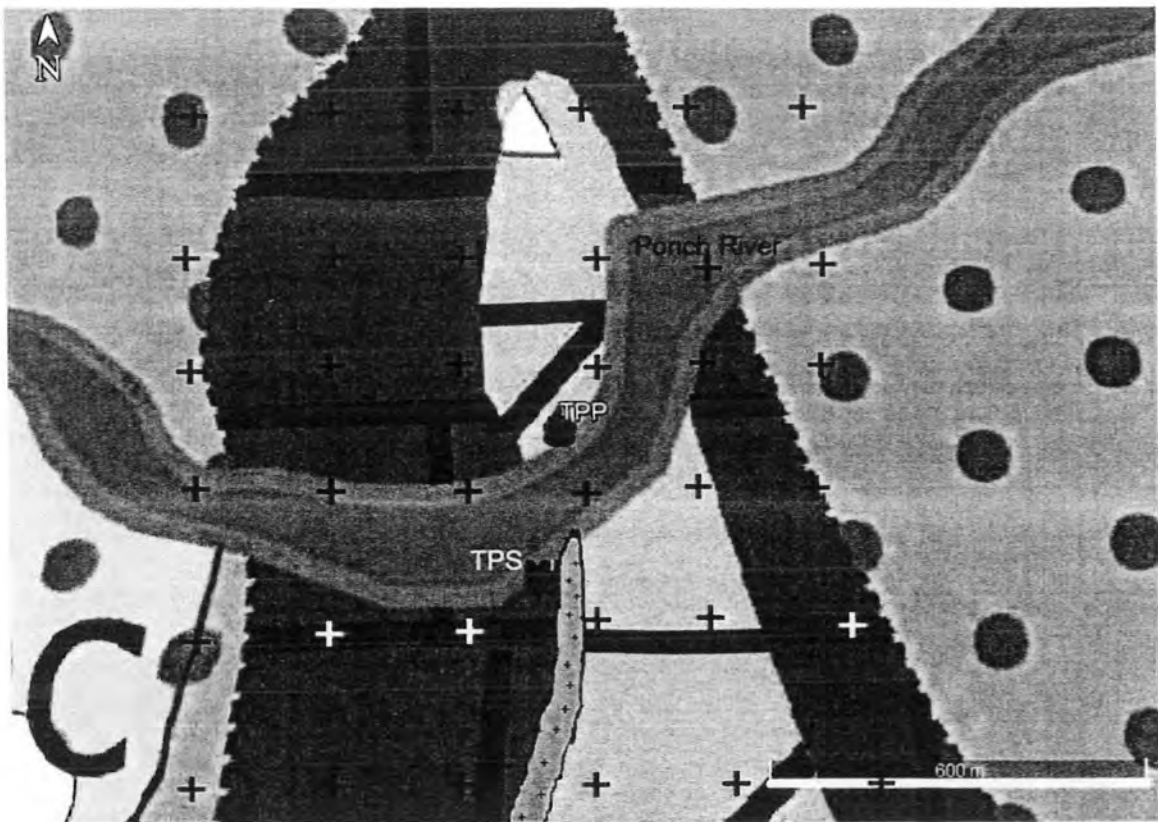
RESULTS AND DISCUSSIONS

4.1 Field Observations

The study area (i.e., Tattapani hot springs) occurs on the gravely bank of Ponch River at Tattapani town, near Kotli, Kashmir (NE Pakistan). A surface manifestation occurs on two sites named as TPP (Primary site, on north bank of river containing 5 hot springs) and TPS (Secondary Site, on south bank of river containing 2 hot springs).

Field observations were carried out with the help of geological map and exposed outcrops. Study area is an anticline and is the northern most part of 28 km long NW-SE trending Tattapani anticline (previously called Tattapani-Karela anticline). Stratigraphy of the area comprises from Cambrian to Recent rock formations. Stromatolite bearing Muzaffarabad formation is exposed in the core of anticline, with its quartzite member along flanks. The formation is dolomitized and fractured. Muzaffarabad formation is overlain by shales of Palaeocene Patala formation. Their contact is marked by an unconformity. Eocene rocks like Margalla Hill Limestone, Chorgali formation and Kuldana formation were not mapped by GSP sheet 43/14, were observed on both flanks on Tattapani anticline. However, the contact in between Palaeocene-Eocene rocks was not clear. Murree formation (Miocene) overlays older rocks and is exposed in region around the flanks of anticline.

Magmatic intrusion was observed along the exposed carbonate succession near TPS (Figure 4.1). Intrusive body was sandwiched between quartzite of Muzaffarabad formation and shales of Patala formation. The intrusive rocks were medium to coarse grain and dark bluish grey to greenish grey in color. The weathering color is yellowish to light grey. Rocks were mostly altered and indicated effects of thermal fluids. Similar intrusive bodies were reported towards SE along the northern flank of Tattapani anticline (Ashraf et al., 1983).








- | | | | |
|---|---|---|-------------------------------------|
|  | Mirpur Conglomerate |  | Basic Intrusion |
|  | Murree Formation | | TPP = Primary site of Hot Springs |
|  | Paleocene-Eocene (Shales with interbedded Limestone) | | TPS = Secondary site of Hot Springs |
|  | Muzaffarbad Formation | | + Radon Sampling Points |

Figure 4.1 Geological map of study area showing location of hot springs and radon sampling points along with intrusive body observed in field study.

4.2 Soil Gas Radon Emissions

Radon concentration was measured with RAD 7 at 36 locations in a grid pattern. Grab samples were taken comprising of a single run with 4 cycles and each cycle having a time period of 5 minutes. Mean radon concentration was calculated averaging the radon concentration measured in all four cycles using following equation;

$$^{222}\text{Rn} (\text{Bq}/\text{m}^{-3}) = \frac{C1 + C2 + C3 + C4}{4}$$

Where;

C1, C2, C3 and C4 are radon concentrations of each cycle respectively.

Concentration of radon in soil at 36 locations of the study area have been calculated and presented in Table 1 along with geographic coordinates and exposed geology. Out of 36 sample locations, 6 points were located on river deposited loose gravel, 7 on shaly rocks, 7 on sandstone of Murree formation, 4 on carbonates of Muzaffarabad Formation and 12 on thick soil covering the underlying rocks.

Radon concentration varied between 2.1 to 29.5 kBq m⁻³ with an average of 7.6 kBq m⁻³. Concentration of radon was highest at sampling point A3 while lowest at C5. Sampling points like A3, F3, B3 and F4 gave anomalous values relative to all other locations (Table 1). Radon anomalies are generally controlled by factors like rock/soil emanation, rock movements and climatic geographies (Mogro Campero and Fleischer, 1977). Generally, quantity of radon released from the crust into the atmosphere is relatively less as revealed from most of sampling points. However, remarkably elevated quantities of radon could be discharged over faults, geothermal zones (in present case), uranium mines and volcanic regions (Nishimura and Katsura, 1990).

Radon concentration is found quite low at sample points located on or near the river bank. Gravel deposited along the bank of river was not consolidated, so the large interconnected pore space between the sediments provide the pathways for surface air to dilute the gases escaping from the subsurface (Table 1).

A contour map was generated using radon concentration values and geographic coordinates. Two anomalies generated quite opposite to each other, i.e. one in the south and one in north as shown in Figure 4.2. However, an N-S trending anomalous zone could be interpreted if both anomalies are joined together. The N-S trending anomalous zone happens to be just above the contact between Muzaffarabad and Patala formations where an igneous intrusion was also observed near TPS (Figure 4.1). Radon out-gassing in crust is controlled by fractures and their irregular distribution (Sac et al., 2011). Radon after release, migrates upward, while its concentration and upward migration is controlled by factors such as; porosity, granulation, humidity, atmospheric pressure, micro-cracks, surface winds etc., (Toutain and Baubron, 1999). The possible interpretation for these anomalous zones could be presence of possible pathways along the contact for the movement of fluids from depth to the surface.

Data from six traverse lines of grid (A,B,C,D,E and F) that run across the Tattapani anticline was plotted to get an idea about effect of lithological changes on the radon concentration as shown in Figure 4.3. Radon concentrations in soil analyzed at surface conditions were found to be reliant on upon various factors: the rock/soil emanation (Morawska and Phillips, 1993), the flow of the carrier gas (Ball et al., 1991) and the permeability of the host rock. Increase in radon in Figure 4.3 could be associated with hot gases escaping from sub-surface towards hot springs with radon concentration usually rising with water temperature, although, increasing temperature decreases solubility of radon. Shales of Patala formation due to high permeability have prominent radon concentration, however the high peaks of radon concentration are more prominent towards shale exposed on the left limb of anticline (Figure 4.3), the possible interpretation could be the presence of a subsurface heat source along shale and carbonate contact, for which radon along with other gases is following a direct escape route.

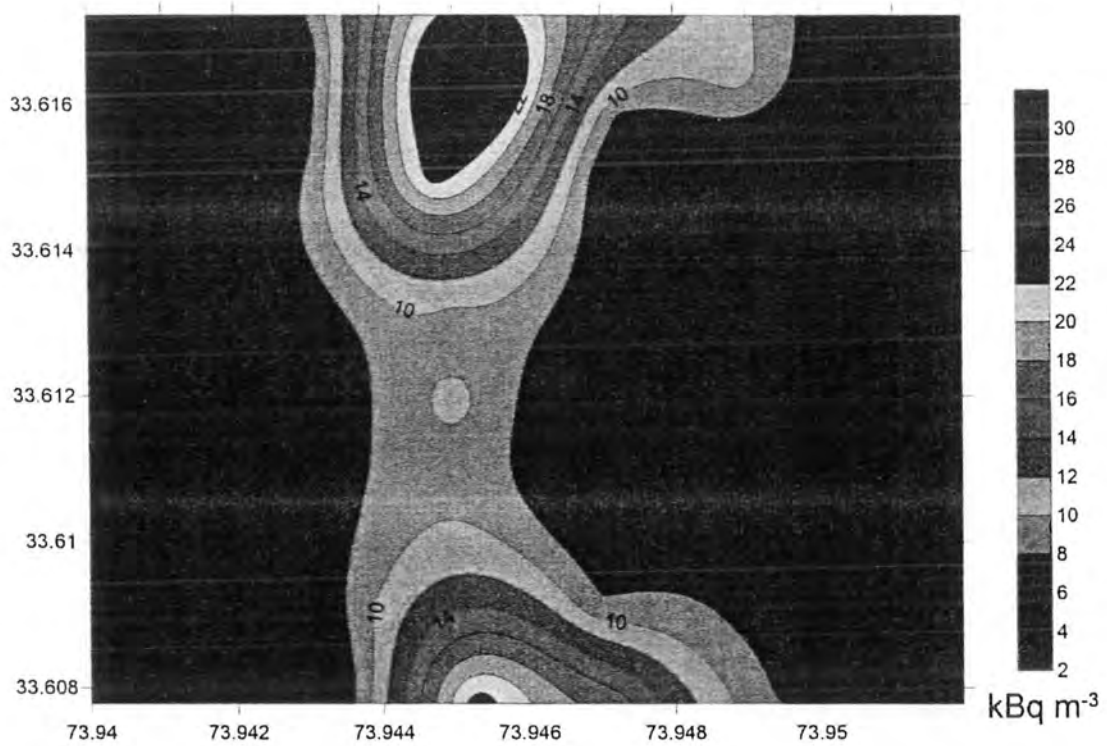


Figure 4.2 Contour map showing spatial variability of radon concentration over the study area

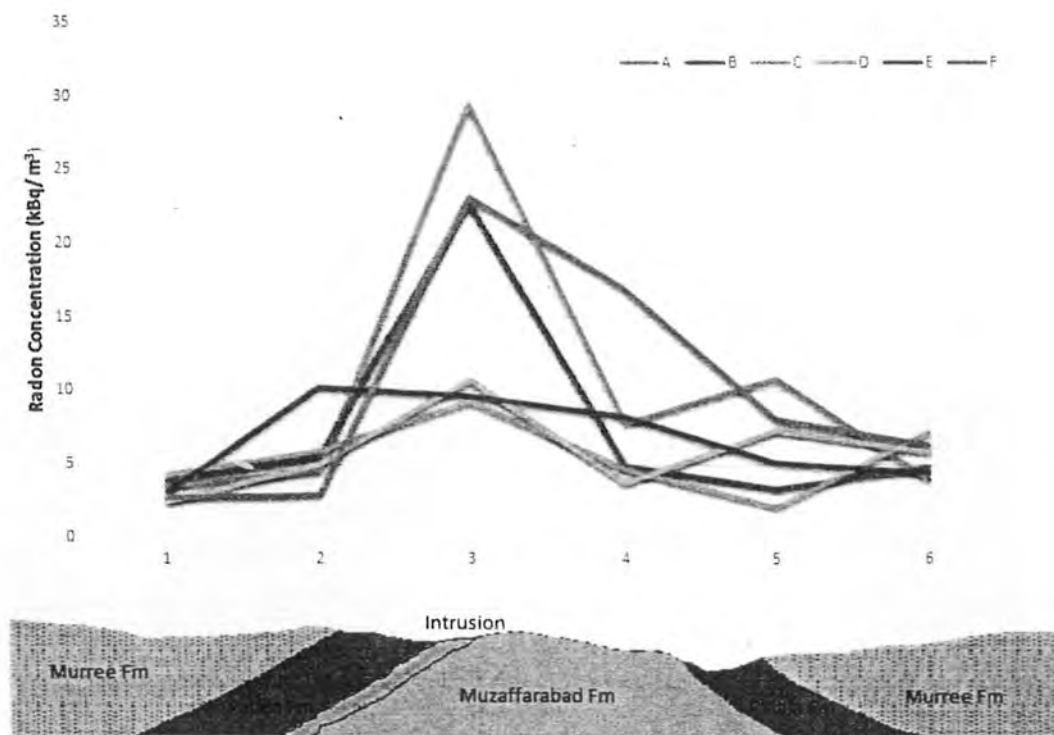


Figure 4.3 Behavior of soil gas radon concentration over different lithologies along 6 traverses of grid moving across the Tattapani anticline in E-W direction.

4.3 Physical Characteristics of Thermal Water

A total of six hot springs were selected for physical measurements. i.e. 5 from TPP and 1 from TPS. Besides this, water samples from nearby river, open well and fresh water spring were also taken to analyze their physical characteristics. The results of the physical analyses of water samples from study area are shown in Table 2. Hot spring waters were slightly acidic with pH ranging 6.62 to 6.69, while temperatures ranged from a low of 55.9°C (Tps-1) to a high of 60.8°C (Tpp-5). Flow rates were variable at each hot spring; vents with larger discharges usually had the highest temperatures. Flow rates of hot springs varied between 3.6 to 15.6 liters per second. Electrical conductivity and total dissolved solids values for hot springs ranged from 1120 to 1260 $\mu\text{S}/\text{cm}$ (micro Siemens per cm) and 740 to 810 ppm respectively.

Water samples other than hot springs were slightly alkaline with quite less values of EC, TDS and temperature. Open well and fresh water sample from cold spring gave relatively higher values of EC and TDS from river samples because they have time to interact with rocks to dissolve the minerals. It was also noted that open well sample (Tpp-W) was having quite abnormal values to be a fresh water, probable explanation was mixing with thermal water and high microbial activity in the well.

4.4 Chemical Composition of Hot springs

Major compositions of a hydrothermal solution based on anions concentrations comprise of chloride (Cl^-), sulfate (SO_4^{2-}) and bicarbonate (HCO_3^-). Because of its unreactive properties, chloride water is mostly used as an indicator of a deep fluid source. The sulfate water originates from the oxidation process of hydrogen sulphide (H_2S) from a steam condensation by cooler waters at shallower depth. The bicarbonate water in a geothermal system is due to absorptions of carbon dioxide (CO_2) and a steam condensation into cooler groundwater (Hedenquist, 1990), which commonly occurs at the peripheral area of a geothermal system i.e. outflow zone (Hochstein & Browne, 2000). In this study, the hot springs have relatively higher proportion of bicarbonate than sulfate and chloride and thus classified as bicarbonate waters. Ternary plot based on major anions (Cl^- , SO_4^{2-} , and HCO_3^-) shows that Tattapani hot springs are bicarbonate type (Figure 4.4).

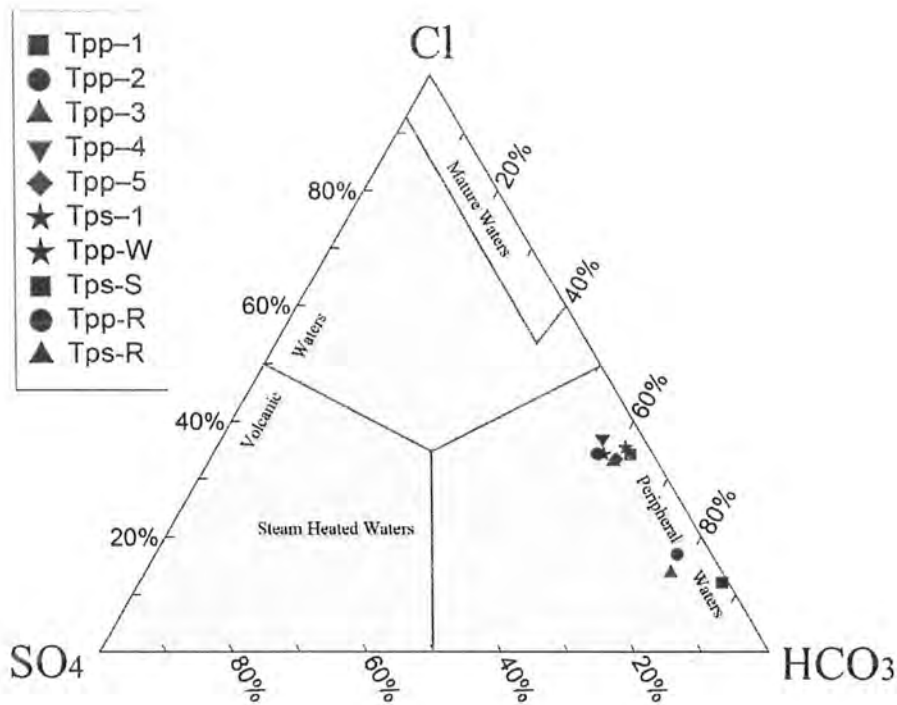


Figure 4.4 Cl-SO₄-HCO₃ ternary diagram (after Giggenbach and Goguel, 1989) showing that Tattapani hot springs are bicarbonate type.

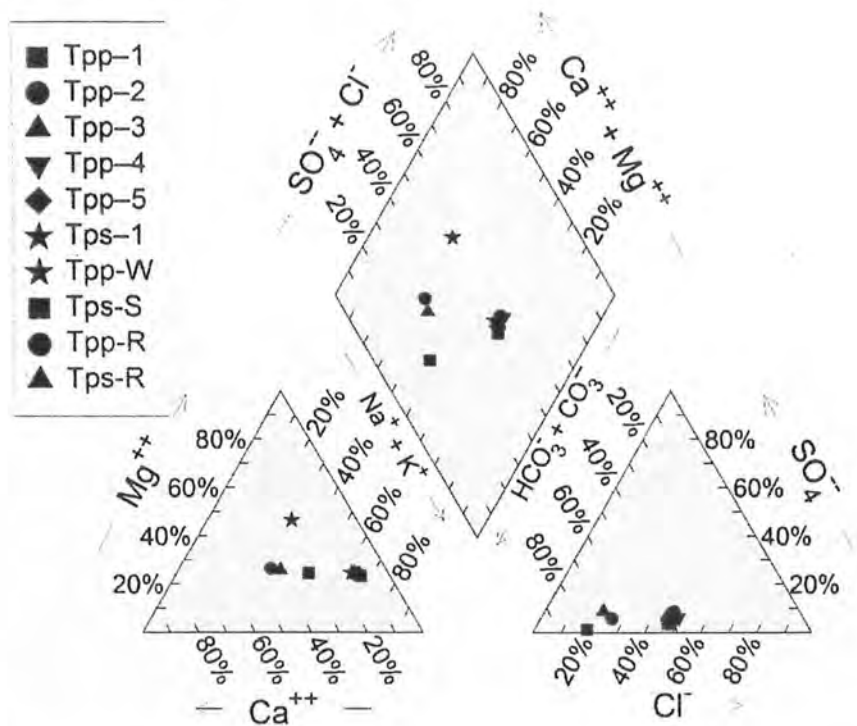


Figure 4.5 Piper plot showing the distinctive chemical nature of thermal water of Tattapani area.

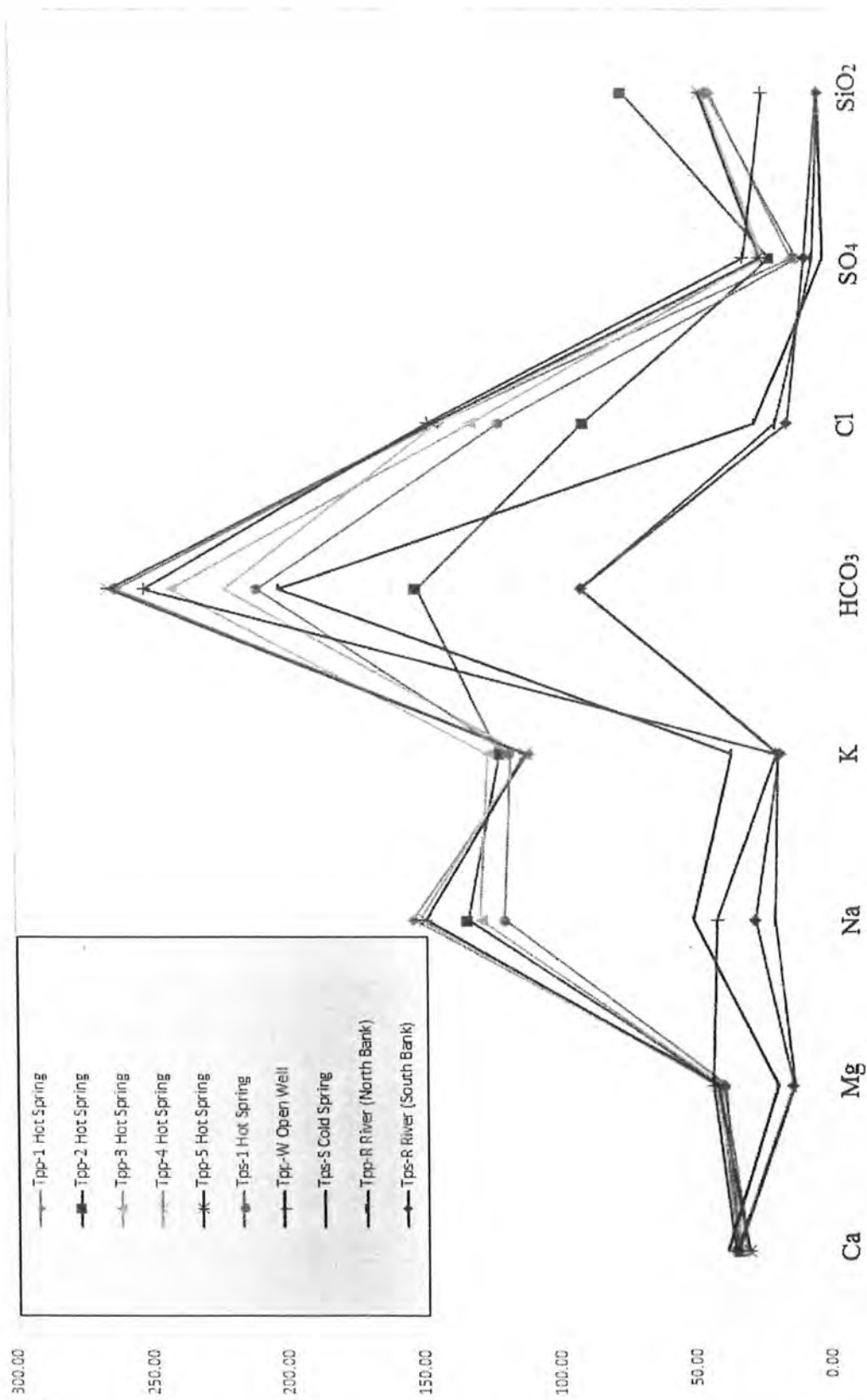


Figure 4.6 Schoeller plot for concentration of major ionic species (ppm) in water samples collected from Tattapani area.

The major cations of a hydrothermal solution comprises of Na, K, Mg, Ca (Henley 1984; Giggenbach, 1997; Marini, 2000). The concentration of these cations within a solution is controlled by equilibration and dissolutions processes of the fluid and rock, as well as by the compositions of the host rock. The condition of equilibration, which is called an equilibrium state, represents the reaction condition in which no further ion exchange occurs. In such an equilibrium state, the amount of a product and the reactant are shown in an equal amount (Fournier, 1989). In the context of a geothermal system, an equilibration process occurs in a high temperature system (Giggenbach, 1997); whereas a dissolution process occurs in a low temperature system. Tattapani hot springs are dominated by cations of alkali metals (Na and K) as shown by Piper plot in figure 4.5. Water samples other than hot springs have relative high concentrations of Ca and Mg. Based on Piper plot (Figure 4.5) Tattapani hot spring can be classified as Na-K-HCO₃, while the water from open well can be classified as Ca-Mg-SO₄-Cl. All other water samples are alkali bicarbonate type.

Schoeller plot (Figure 4.6) is used to get an idea of relative concentrations of major components in water. The high sodium and potassium in the aqueous phase probably results from the dissolution of plagioclase feldspar present in igneous intrusion in the area. Another potential source is from cation exchange with clays found in the sedimentary interbeds present in the area. At high temperatures ($T^{\circ}\text{C} > 120^{\circ}\text{C}$) K equilibria is controlled by temperature dependent mineral-fluid reactions, while at lower temperatures K maybe incorporated into secondary clay minerals (Savage et al., 1993). Ca is released by the dissolution of plagioclase feldspar and carbonates is then controlled by precipitation of minerals exhibiting retrograde solubility (e.g. calcite, anhydrite). Calcite, aragonite, and dolomite are significantly more soluble in water than plagioclase feldspar; therefore, the limestone is the most likely source due to solubility and dissolution reactions. The Mg content in thermal waters is typically very low, however presence of dolomitized limestone in the area may be the reason for its noticeable concentration indicating that a shallow dissolution is occurring (Reyes et al., 2010) (known as 'immature' waters of Giggenbach, 1988). Because the concentration of Cl⁻ is not controlled by mineral solubility (Arnorsson, 2000; Browne & Rodger, 2006), its presence in spring waters represents the contribution from a deep fluid source (Fournier, 1979; Reyes et al., 2010). Deep fluid source might ascend to shallower depth through permeable faults system.

4.5 Geothermometry

Geothermometry is a temperature estimation method which considers the relative concentrations of cations (e.g., Na-K-Ca, Na-K, K-Mg) and the total dissolved silica (e.g. amorphous silica, chalcedony, or quartz) from a thermal spring sample (Fournier, 1981). The assumptions of a Geothermometry method are (Fournier, 1977); 1) the equilibrium state of fluid and rock is achieved; 2) there are neither re-equilibration states nor fluid mixing occurring during the fluid flow; 3) a temperature-dependent reaction involving rock and fluid occur within the system. In a non-equilibrium state, the cations geothermometer would not represent the actual temperature since the reaction is in imbalance.

4.5.1 Silica Geothermometry

Silica geothermometer is used based on their solubility on the solution, which is temperature dependent. The assumptions of silica geothermometer are (Fournier, 1989); 1) equilibrium of fluid and quartz occurs; 2) fluid mixing does not occur during ascending fluid to shallower depth. Silica may occur in various forms or polymorphs in geothermal areas: quartz, chalcedony, cristobalite and amorphous silica (Ellis and Mahon, 1977). Each of the SiO₂ phases has a distinct solubility with respect to temperature. Among the three silica polymorphs, chalcedony has very fine crystal grains in providing a larger surface energy than quartz; hence, their solubility is higher than quartz, particularly within a medium temperature system (< 120°C) (Fournier, 1989). The quartz itself is more soluble in a high temperature system.

Speciation of thermal waters with the program GWB (Geochemist Workbench) yielded calculated saturation indexes for the various silica minerals. The waters are found to be at near equilibrium respecting quartz and undersaturated with respect to amorphous silica. The quartz concentrations are controlled by adiabatic (max steam loss) or conductive (no steam loss) cooling processes. Reservoir temperatures on basis of quartz (conductive) geothermometer (Fournier, 1977) are 96.01 to 122.53°C, while 97.54 to 120.31°C on basis quartz (adiabatic) geothermometer by Fournier, 1977 as shown in Figure 4.8. Silica polymorphs or volcanic glass may also control the concentration of silica in solution. Because of the small number of igneous dikes in the field area the cristobalite

geothermometer was not applied in this investigation. The amorphous silica geothermometer was rejected because it yielded temperatures which are well below the temperature of discharge. Results of all silica geothermometers used various authors are presented in Table 4.

4.5.2 Cation Geothermometry

The cation geothermometers are based on the assumption that the last equilibrium state between the fluid and minerals of the host rock is attained (Fournier, 1981, 1991; Giggenbach, 1988, 1991). The major cations of geothermal fluids and rocks are Na, K, Mg, Ca (Giggenbach, 1988). The equilibrium reaction between geothermal fluids and the prevailing rocks, depends on the degree of kinetic mineral dissolution and deposition reactions, vapor loss, dilution and fluid mixing from different sources (Giggenbach, 1988). The formulation of an equilibrium state indicator based on the major cations analysis is introduced by Giggenbach (1988) by means of a four cations Na-K-Mg-Ca.

The results of the Na-K geothermometers (Truesdell, 1976; Fournier, 1979; Tonani, 1980; Arnorsson et al., 1983; Nieva & Neiva, 1987; Giggenbach, 1988) ranges from 443.90 – 845.26 °C as shown in (Table 5). Results obtained from Na-K geothermometers are too high, which could not be possible in this system. Such high source temperatures might imply that an equilibrium has not yet attained in case of Na-K exchange reactions at reservoir conditions indicating a non-equilibrium state of fluid and rock due to a dissolution process rather than equilibration. Therefore, a cation geothermometer such as Na-would not represent deep temperature estimation (Giggenbach, 1988; Reyes et al, 2010; Hochstein et al., 2013). However, some cations among major four (Na-K-Mg-Ca) might still reach an equilibrium, i.e. K-Mg, which requires a shorter time to reach equilibrium than Na-K (Fournier, 1989).

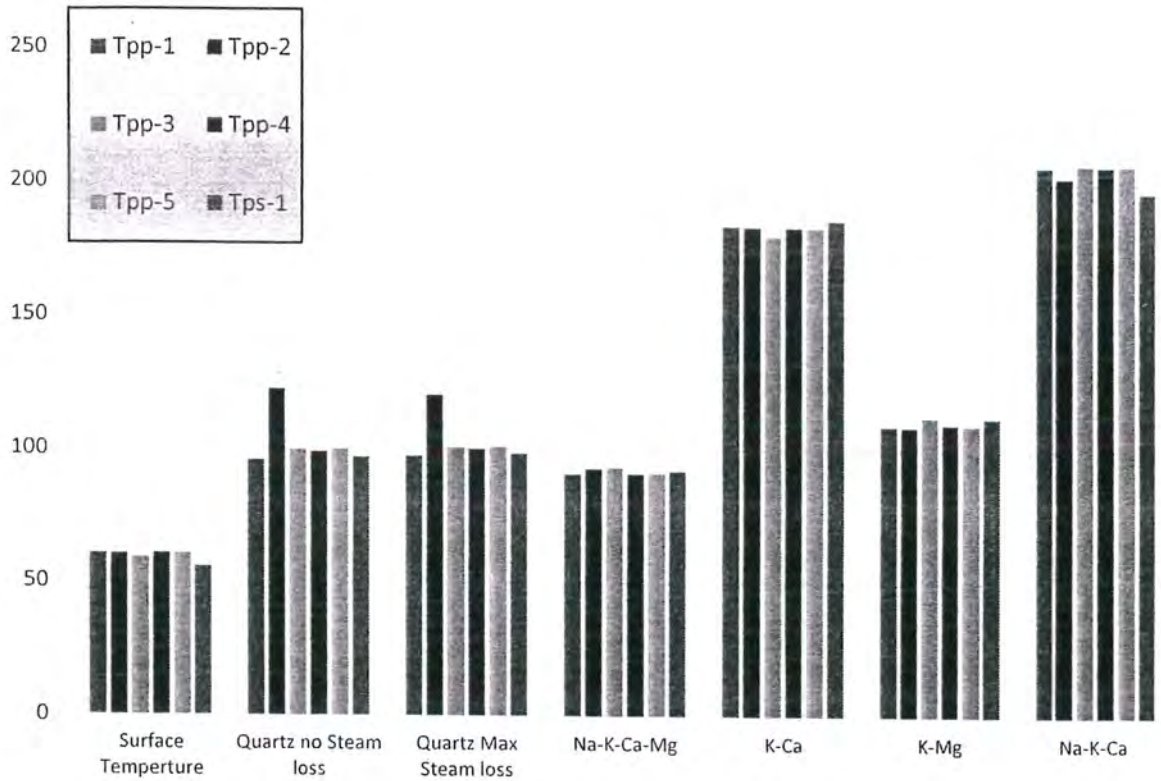


Figure 4.7 Bar chart showing reservoir temperatures (°C) calculated from selected geothermometers.

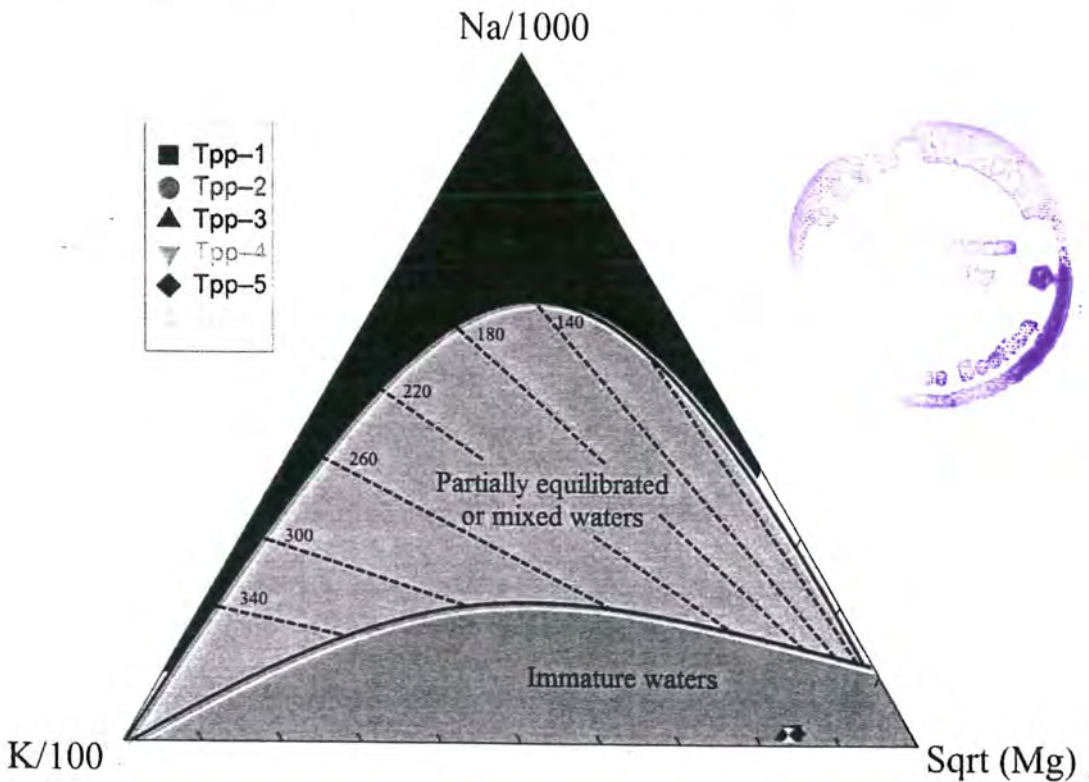


Figure 4.8 Na-K-Mg Ternary plot (after Giggenbach, 1988) used to determine reservoir temperature and to recognize equilibrated water suitable for geothermometry

The result temperatures of K-Mg geothermometer (Giggenbach, 1983) calculation from hot springs of Tattapani are 109.22–112.62 °C (Figure 4.7; Table 5). Reservoir temperatures calculated using K-Ca geothermometer (Tonani, 1980) are higher ranging between 180.18–186.16°C, while Na-K-Mg-Ca geothermometer gave results ranging between 90.96 to 93.45 °C as shown in Figure 4.7. Na-K-Mg Ternary Diagram (Giggenbach, 1988) indicated that thermal waters are immature (Figure 4.8) because system is in non-equilibrium state with respect to Na-K-Mg and a dissolution process may be dominating the system instead of an equilibration process (Reyes et al., 2010).

4.6 Origin of Thermal Waters

Most of the geothermal water has depleted oxygen and lies at the proximity of the meteoric water line (Craig, 1963), suggesting that geothermal water originates mainly from meteoric water (Ellis and Mahon, 1977; Truesdell and Hulston, 1980). Rock is mostly consisting of oxygen and its isotope can be exchanged with the circulating fluid (Craig, 1963; Truesdell and Hulston, 1980; Blattner 1985). The composition of oxygen stable isotopes is dependent on the isotope fractionation which occurs due to isotope exchange reactions, mass differences from chemical reactions, and physical processes. These physical processes are evaporation, boiling condition, and fluid mixing. The isotope fractionation can be different depending on the fluid origin, i.e. rain water, sea water, and magmatic water (Faure, 1991). The elevation where waters are located also affects the concentration of the oxygen stable isotope. The water from a higher elevation would have a lower oxygen isotope because lower precipitation commonly occurs in higher elevations where the temperature is lower (Clark and Fritz, 1997).

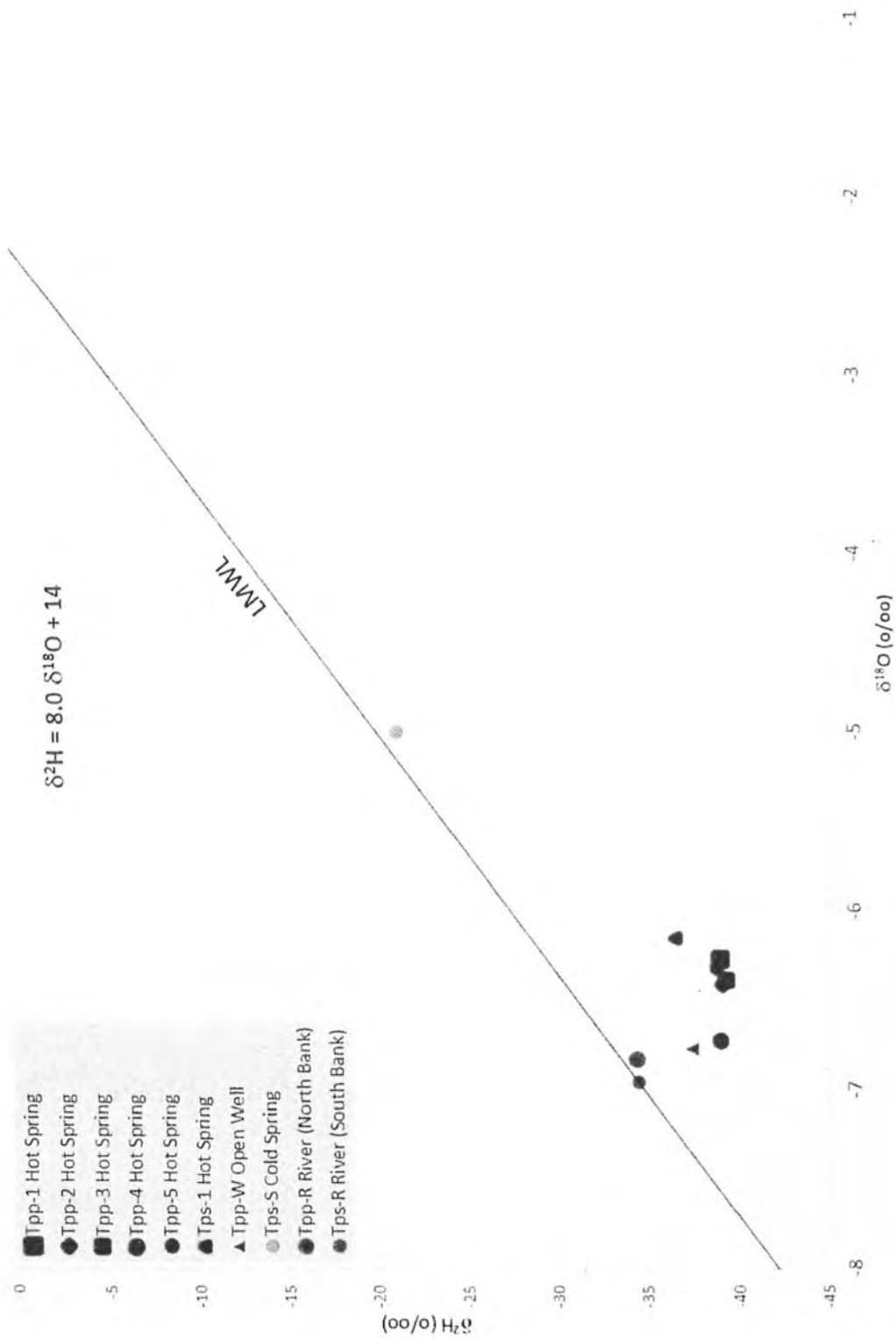


Figure 4.9 $\delta^2\text{H}$ vs. $\delta^{18}\text{O}$ plot constructed from delta values of oxygen and hydrogen relative to VSMOW.

Isotopic data (Table 6) can be used to distinguish between the three probable origin of geothermal water i.e. magmatic, oceanic and meteoric. Ranges of $\delta^{18}\text{O}$ and $\delta^2\text{H}$ of all the sampled hot springs of Tattapani are -6.72 to -6.15‰ and -39.37 to -36.57‰ respectively. This data eliminates the possibility of presence of any significant contribution from magmatic origin water which generally has $\delta^{18}\text{O}$: $+6$ to $+9\text{‰}$ and $\delta^2\text{H}$: -40 to -80‰ (Pearson and Rightmire, 1980; Giggenbach, 1992). Normally the oceans have $\delta^{18}\text{O}$ & $\delta^2\text{H}$ about 0‰ (VSMOW). Depleted values of $\delta^2\text{H}$ and $\delta^{18}\text{O}$ rule out contribution of oceanic water. These values lie close to local meteoric water line of this area (Ahmad et. al., 2007), indicating possibility of recharge from meteoric water. $\delta^2\text{H}$ and $\delta^{18}\text{O}$ of open well lie quite close to values of thermal spring values (Figure 4.9), the possible explanation could be that, well is being recharged by the seepage of deep water of hot springs.

Figure 4.9 indicates the possible source of recharge of meteoric water could be same due to their position on $\delta^2\text{H}$ vs. $\delta^{18}\text{O}$ plot. However, ^{18}O shift due to exchange between water and rocks at higher temperatures as a result of which water of hot springs seems less depleted in ^{18}O . It seems that origin of all the geothermal springs is meteoric water recharging from the rains and snow melts, most probably in the north of the area.

4.7 Residence Time

Tritium concentrations are useful for determining the age of water because tritium is readily incorporated into water molecules in the atmosphere, is rapidly removed via precipitation, and was not present in the atmosphere in large amounts until thermonuclear bomb testing began in 1952 (Mazor, 1991). Tritium's short half-life of 12.34 years makes tritium useful for qualitatively estimating residence time of water as being older or younger than atmospheric thermonuclear bomb testing.

Tritium content of the thermal waters of Tattapani area is about zero (less than detection limits i.e. 0.7 TU). Exact input data of tritium is not needed for dating if no tritium is found in thermal water because, whatever the values may be, it would decay to the level of detection limit within 60 years. Hence on the basis obtained tritium data, it can be inferred that these thermal waters were recharged prior to the start of nuclear weapon testing (1952) (Clark and Fritz, 1997). Tritium of the shallow open wells in the area is also less than the detection limit showing residence time more than 60 years, whereas cold spring

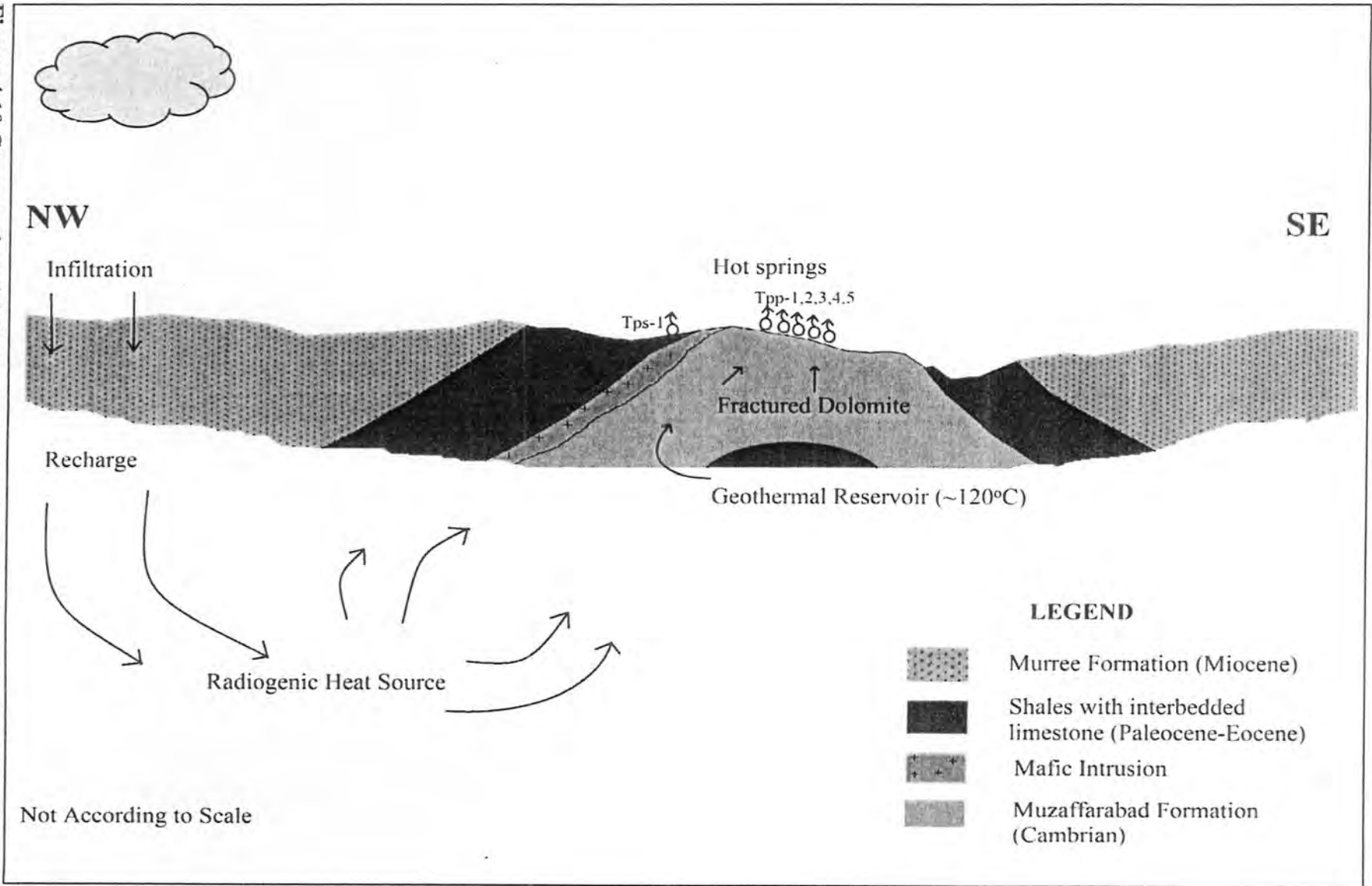
has considerable tritium (7.95 TU), which indicates significant contribution of young water in the recharge. Similarly, no tritium was found in Tattapani geothermal springs indicating residence time more than 60 years (Ahmad et. al., 2008).

4.8 Conceptual Model

The generalized conceptual model (Figure 4.10) for Tattapani hot springs shows cold, dense, meteoric water circulating down through permeable zone (faults and fractures) in the mountains, becoming heated by the radiogenic heat emitted from subsurface igneous intrusion, accumulating in thermal reservoir at depth and circulating back up to the surface along either by fractures present in carbonates or highly permeable shales.

Results of this study also suggest that the probable source of recharge is meteoric water which could be either in the form of snow melt or rain in the northern high altitude regions. This water is infiltrated to a depth where it is heated by the hot sub-surface magmatic body. The anticline structure present in the area provides an excellent structural trap for the hot water. Hot water from the subsurface reservoir travels to the surface through the pathways provided by fractured dolomitized limestone (Muzaffarabad Formation) and permeable shale (Patala Formation).

Figure 4.10 Conceptual model of the geothermal system in Tattapani area is shown on a geological cross section in NW-SE direction.



CHAPTER 5

CONCLUSIONS AND RECOMMENDATIONS

5.1 Conclusions

The purpose of this project was to delineate zones of high radon emissions and to evaluate hot spring waters using hydrogeochemical methods. Soil gas radon survey conducted at Tattapani area provided an overview of soil gas radon distribution patterns produced by underlying system. Anomalous radon concentration (10 to 33 kBq m⁻³) was observed over the possible contact between Cambrian and Cenozoic rocks, which act as permeable pathway for subsurface gases.

Tattapani hot springs are slightly acidic with surface temperatures between 55.9-60.8°C. Based on major ion analysis of water, Tattapani hot spring are classified as sodium bicarbonate type. The fluid characteristic of Tattapani hot springs indicates an up-flow from a low temperature geothermal system with no contribution of magmatic water. Estimates of subsurface temperatures for each of the six hot spring has shown that the subsurface reservoir temperatures are relatively low - between 110 and 140°C on basis of silica and cation geothermometers. However, the non-equilibration of fluid-rock is occurring, although there is an indication of some minor deep derived fluid within the geothermal system. Conduction through water-rock interaction is the dominant process for cooling of thermal waters.

Studies of isotopic ratios of meteoric and thermal waters from the Tattapani area found no evidence for the presence of a magmatic component in any of thermal waters. To the contrary, isotopic data in thermal waters suggest that the waters are entirely of meteoric origin. Probable source of recharge is meteoric water (rains and/or snow-melt at higher altitude) from the mountains to the north of the area. Tritium content of the hot springs and shallow open well in the area is zero (less than the detection limit) showing that that these waters were recharges before the thermonuclear testing began in 1952, so the residence time more than 60 years.

In conclusion, it appears that the hot springs in Tattapani area, being immature and low enthalpy system, does not look promising for the development of geothermal power. Although the presence of a magmatic heat source at depth could not be established through previous studies, but based upon the results of current study, an igneous source emitting radiogenic heat at depth is the most likely explanation of a geothermal system in this area.

5.2 Recommendations

Following are some meaningful recommendations and suggestion based on current study;

- This study should be considered as preliminary, and further geophysical techniques (like gravity and magnetic survey) should be incorporated for better understanding of sub-surface dynamics of the area.
- C-14 isotope dating should be carried out to calculate the residence time of thermal waters.
- Tattapani hot springs, being a low enthalpy system should be used for domestic and commercial purposes like spa, fish farming, space heating etc.
- An integrated study like this, would be useful to study other geothermal fields in Pakistan, especially where no surface manifestations are present (blind geothermal systems).

REFERENCES

- Aadil, N., & ur Rehman, T. (2013). Stratigraphy and structure of Sarda, Manil, Changpur and Naghal areas, district Kotli, Jammu & Kashmir. *Journal of the Geological Society of India*, 82 (6), 639-648.
- Ahmad, M., Akram, W., Ahmad, N., Tasneem, M. A., Rafiq, M., & Latif, Z. (2002). Assessment of reservoir temperatures of thermal springs of the northern areas of Pakistan by chemical and isotope geothermometry. *Geothermics*, 31(5), 613-631.
- Ahmad, M., Akram, W., Hussain, S. D., Sajjad, M. I., & Zafar, M. S. (2001). Origin and subsurface history of geothermal water of Murtazabad area, Pakistan-isotopic evidence. *Applied Radiation and Isotopes*, 55(5), 731-736.
- Ahmad, M., Rafiq, M., Iqbal, N., Akram, W., Tasneem, M. A., & All, M. (2005). Investigation of Major Geothermal Fields of Pakistan Using Isotope and Chemical Techniques. *Proceedings World Geothermal Congress. Antalya, Turkey* 1-10.
- Ahmad, M., Rafique, M., Iqbal, N., & Fazil, M. (2009). *Investigation of origin, subsurface processes and reservoir temperature of geothermal springs around Koh-i-Sultan volcano, Chagai, Pakistan*. Pakistan Institute of Nuclear Science and Technology, Islamabad (Pakistan). Isotope Application Division. PINSTECH/RIAD-210.
- Ahmad, M., Rafique, M., Tariq, J. A., Choudhry, M. A., & Hussain, Q. M. (2008). *Isotope and chemical investigation of geothermal springs and thermal water produced by oil wells in Potwar area, Pakistan*. Pakistan Institute of Nuclear Science and Technology, Islamabad (Pakistan). Isotope Application Division. PINSTECH/RIAD-206.
- Ahmad, M., Sheikh, M. R., Akram, W., Tasneem, M. A., Iqbal, N., & Latif, Z. (2007). *Investigation of geothermal fields in himalayan range in pakistan using isotope and chemical techniques*. Pakistan Inst. of Nuclear Science and Technology, Islamabad (Pakistan). Isotope Application Div. PINSTECH/RIAD-202.
- Ahmad, M., Tasneem, M. A., Akram, W., Hussain, S. D., Zafar, M. S., & Sajjad, M. I. (2000). Isotopic investigations of Tatta Pani and Tato thermal springs: insights to their origin, age and subsurface history. *JSNM (Nuclear Science Journal of Malaysia)*, 18(2).
- American Public Health Association. (2005). Standard methods for the examination of water and wastewater. *American Public Health Association (APHA): Washington, DC, USA*.
- AOAC (2000). Official methods of analysis of AOAC international. 17th edition, William, H.(edt). Maryland, USA. Vol. 1. Method 977.15.
- Arnórsson, S. (2000). Isotopic and chemical techniques in geothermal exploration, development and use. *International Atomic Energy Agency*, 109-111.

- Arnorsson, S., Gunnlaugsson, E., & Svavarsson, H. (1983). The chemistry of geothermal waters in Iceland. III. Chemical geothermometry in geothermal investigations. *Geochimica et Cosmochimica Acta*, 47(3), 567-577.
- Ashraf, M., Chaudhry, M. N., & Malik, R. H. (1986). Bituminous/anthracitic coal of Kotli District, Azad Kashmir. *Kashmir Journal of Geology*, 4, 1-14.
- Ashraf, M., Chaudhry, M. N., & Qureshi, K. A. (1983). Stratigraphy of Kotli area of Azad Kashmir and its correlation with standard type areas of Pakistan. *Kashmir Jour. Geol.*, 1(1), 19-30.
- Bakht, M. S. (2000). An Overview of Geothermal Resources of Pakistan. *Proceedings of the World Geothermal Congress, Kyushu-Tohoku, Japan.* 77-83.
- Bakr, M. A. (1965). Thermal springs of Pakistan. *Pakistan Geol. Surv. Rec.*, 16.
- Balcázar M., López Martínez A., Huerta M., Flores Ruíz J.H., & Peña P., (2011). Use of Environmental Radioactive Isotopes in Geothermal Prospecting. *The 17th Pacific Basin Nuclear Conference*, Instituto Nacional de Investigaciones Nucleares, Mexico.
- Balcazar, M., Gonzalez, E., Ortega, M., & Flores, J. H. (1993). Geothermal energy prospecting in El Salvador. *Nuclear Tracks and Radiation Measurements*, 22(1), 273-276.
- Balcazar, M., Lopez, A., Flores, M., & Huerta, M. (2014). Natural radiation contribution to renewable energy searching. *International Symposium on Solid State Dosimetry (ISSSD)*, Cusco, Peru. 29 p.
- Ball, T. K., Cameron, D. G., Colman, T. B., & Roberts, P. D. (1991). Behaviour of radon in the geological environment: a review. *Quarterly Journal of Engineering Geology and Hydrogeology*, 24(2), 169-182.
- Blattner, P. (1985). Isotope shift data and the natural evolution of geothermal systems. *Chemical geology*, 49(1), 187-203.
- Browne, P. R., & Rodgers, K. A. (2006). Occurrence and significance of anomalous chloride waters at the Orakei Korako geothermal field, Taupo Volcanic Zone, New Zealand. *Geothermics*, 35(3), 211-220.
- Clark, I.D., and Fritz, P., (1997). *Environmental isotopes in hydrogeology*: Boca Raton, Florida, CRC Press, 328 p.
- Coleman, M. L., Shepherd, T. J., Durham, J. J., Rouse, J. E., & Moore, G. R. (1982). Reduction of water with zinc for hydrogen isotope analysis. *Analytical Chemistry*, 54(6), 993-995.
- Cox, M. E. (1980). Ground radon survey of a geothermal area in Hawaii. *Geophysical Research Letters*, 7(4), 283-286.
- Craig, H. (1963). The isotopic geochemistry of water and carbon in geothermal areas. *Nuclear Geology on Geothermal Areas*, 17-53.

- DiPietro, J. A., and K. R. Pogue (2004), Tectonostratigraphic subdivisions of the Himalaya: A view from the west, *Tectonics*, 23, TC5001, doi:10.1029/2003TC001554.
- Duddridge, G. A. (1994). Observations on soil gas variations in the Bovey Basin. *Proceedings-Ussher Society*, 8, 331-331.
- Ellis, A.J. & Mahon, W.A.J. (1977). *Chemistry and geothermal systems*. Academic Press, New York, 392 pp.
- Epstein, S., & Mayeda, T. (1953). Variation of O 18 content of waters from natural sources. *Geochimica et cosmochimica acta*, 4(5), 213-224.
- Faure, G. (1991). *Principles and applications of inorganic geochemistry: a comprehensive textbook for geology students*. United States of America: Macmillan Publishing Company, 626 pp.
- Fleischer, R. L., (1988). Radon in the environment-opportunities and hazards. *Nuclear Tracks and Radiation Measurements*, 14, 421-435.
- Florkowski, T. (1981). Low-level tritium assay in water samples by electrolytic enrichment and liquid-scintillation counting in the IAEA laboratory. In *Methods of low-level counting and spectrometry*, International atomic Energy Agency, Vienna, 336-357.
- Fournier, R. O. (1977). Chemical geothermometers and mixing models for geothermal systems. *Geothermics*, 5(1), 41-50.
- Fournier, R. O. (1979). Geochemical and hydrologic considerations and the use of enthalpy-chloride diagrams in the prediction of underground conditions in hot-spring systems. *Journal of Volcanology and Geothermal Research*, 5(1), 1-16.
- Fournier, R. O. (1989). *Lectures on geochemical interpretation of hydrothermal waters* (No. 10). UNU Geothermal Training Programme. Iceland, Report 10, 73 pp.
- Fournier, R. O. (1991). Water geothermometers applied to geothermal energy. *Application of Geochemistry in Geothermal Reservoir Development*, Ed Franco D'Amore. Unitar/UNDP, 37-69.
- Fournier, R. O. 1981. Application of water geochemistry to geothermal exploration and reservoir engineering. *Zn L. Rybach and L J F*, 109-143.
- Fu, C., Yang, T. F., Walia, V., & Chen, C. (2005). Reconnaissance of soil gas composition over the buried fault and fracture zone in southern Taiwan. *Geochemical Journal Japan*, 39(5), 427-439.
- Giggenbach W. F. & Goguel R. L. (1989). *Collection and analysis of geothermal and volcanic water and gas discharges*, New Zealand DSIR Chemistry Div. Rprt. CD 2401. 81 p.
- Giggenbach, W. F. (1982). Carbon-13 exchange between CO₂ and CH₄ under geothermal conditions. *Geochimica et Cosmochimica Acta*, 46(2), 159-165.

- Giggenbach, W. F. (1988). Geothermal solute equilibria. Derivation of Na-K-Mg-Ca geothermometers. *Geochimica et cosmochimica acta*, 52(12), 2749-2765.
- Giggenbach, W. F. (1991). Chemical techniques in geothermal exploration. *Application of geochemistry in geothermal reservoir development*, 11, 9-144.
- Giggenbach, W. F. (1992). Isotopic shifts in waters from geothermal and volcanic systems along convergent plate boundaries and their origin. *Earth and planetary science letters*, 113(4), 495-510.
- Giggenbach, W. F. (1997). Relative importance of thermodynamic and kinetic processes in governing the chemical and isotopic composition of carbon gases in high-heatflow sedimentary basins. *Geochimica et Cosmochimica Acta*, 61(17), 3763-3785.
- Giggenbach, W. F., & Goguel, R. T. (1988). *Methods for the collection and analysis of geothermal and volcanic water and gas samples*. NZ-DSIR Report, CD 2387, 53 pp.
- Giggenbach, W. F., Gonfiantini, R., Jangi, B. L., & Truesdell, A. H. (1983). Isotopic and chemical composition of Parbati valley geothermal discharges, north-west Himalaya, India. *Geothermics*, 12(2), 199-222.
- Gingrich, J. E. (1984). Radon as a geochemical exploration tool. *Journal of Geochemical Exploration*, 21(1), 19-39.
- Haerudin, N., Munadi, S., & Suryanto, W. (2013). A Soil Gas Radon Survey to Determine Fault at Southern Part of Rajabasa Geothermal Field, Lampung Indonesia. *International Journal of Engineering & Technology*, 13(1), 75-81.
- Hedenquist, J. W. (1990). The thermal and geochemical structure of the Broadlands-Ohaaki geothermal system, New Zealand. *Geothermics*, 19(2), 151-185.
- Henley, R. W. (1984). Chemical structure of geothermal systems. *Economic Geology*, 1, 9-28.
- Hochstein, M. P., & Browne, P. R. (2000). Surface manifestations of geothermal systems with volcanic heat sources. *Encyclopedia of Volcanoes*, 835-855.
- Hochstein, M.P., Zheng, K., Pasvanoglu, S., Vivian-Neal, O., 2013. Advective (Heat Sweep) Geothermal Systems. In: *Proceeding Thirty-Eight Workshop on Geothermal Reservoir Engineering*, Stanford University. SGP-TR-198: 11-13.
- Hussain, A., Yeats, R. S., & Lisa, M. (2009). Geological setting of the 8 October 2005 Kashmir earthquake. *Journal of seismology*, 13(3), 315-325.
- Hussain, S.D., & Asghar, G., (1982). Programme for TI Programmable Calculator for Calculation of ³H Concentration of Water Samples. Pakistan Inst. of Nuclear Science and Technology, Islamabad (Pakistan). Isotope Application Div PINSTECH/RIAD-102.



- Ioannides, K., Papachristodoulou, C., Stamoulis, K., Karamanis, D., Pavlides, S., Chatzipetros, A., & Karakala, E. (2003). Soil gas radon: a tool for exploring active fault zones. *Applied Radiation and Isotopes*, 59(2), 205-213.
- Johnson, B. D., Powell, C. M., & Veevers, J. J. (1976). Spreading history of the eastern Indian Ocean and Greater India's northward flight from Antarctica and Australia. *Geological Society of America Bulletin*, 87(11), 1560-1566.
- Jönsson, G. (1995). Radon gas—where from and what to do?. *Radiation measurements*, 25(1), 537-546.
- Kaneda, H., Nakata, T., Tsutsumi, H., Kondo, H., Sugito, N., Awata, Y., & Kausar, A. B. (2008). Surface rupture of the 2005 Kashmir, Pakistan, earthquake and its active tectonic implications. *Bulletin of the Seismological Society of America*, 98(2), 521-557.
- Karingithi, C., & Wambugu, J. (2010). The geochemistry of Arus and Bogoria geothermal prospects. In *Proceedings of the World Geothermal Congress, Bali, Indonesia*, 25-29.
- Kazmi, A. H. (1979). Active fault systems in Pakistan. *Geodynamics of Pakistan*, 285-294.
- Kendall, C., & Coplen, T. B. (1985). Multi-sample conversion of water to hydrogen by zinc for stable isotope determination. *Analytical Chemistry*, 57(7), 1437-1440.
- Krouse, H. R. (1980). Sulphur isotopes in our environment. *Handbook of environmental isotope geochemistry*, 1, 435-471.
- Lee, J. M., & Kim, G. (2006). A simple and rapid method for analyzing radon in coastal and ground waters using a radon-in-air monitor. *Journal of environmental radioactivity*, 89(3), 219-228.
- López, A., Gutiérrez, L., Razo, A., & Balcázar, M. (1987). Radon mapping for locating geothermal energy sources. *Nuclear Instruments and Methods in Physics Research Section A: Accelerators, Spectrometers, Detectors and Associated Equipment*, 255(1), 426-429.
- Lydekker, R. (1883). The geology of the Kashmir and Chamba territories and the districts of Khasia. *Mem. Geol. Sur. Ind*, 22, 211-24.
- Malinconico, L. L. (1989). Crustal thickness estimates for the western Himalaya. *Geological Society of America Special Papers*, 232, 237-242.
- Maluski, H., & Matte, P. (1984). Ages of alpine tectonometamorphic events in the northwestern Himalaya (northern Pakistan) by $^{39}\text{Ar}/^{40}\text{Ar}$ method. *Tectonics*, 3(1), 1-18.
- Marini, L. (2000). *Geochemical techniques for the exploration and exploitation of geothermal energy*. Dipartimento per lo Studio del Territorio e delle sue Risorse, Università degli Studi di Genova Genova, Italy. 106 pp.

- Mazor, E., (1991). *Applied Chemical and Isotopic Groundwater Hydrology*. Halsted Press, New York, 274 pp.
- Mogro-Campero, A., & Fleischer, R. L. (1977). Subterrestrial fluid convection: a hypothesis for long-distance migration of radon within the earth. *Earth and Planetary Science Letters*, 34(2), 321-325.
- Morawska, L., & Phillips, C. R. (1993). Dependence of the radon emanation coefficient on radium distribution and internal structure of the material. *Geochimica et Cosmochimica Acta*, 57(8), 1783-1797.
- Munir, M. U. H., & Baig, M. S. (2006). Paleogene biostratigraphy of Tattapani, Kotli Azad Kashmir, Northwest sub-Himalayas, Pakistan. *Journal of Himalayan Earth Sciences*. 39, 39-48.
- Neiva, A. M., Neiva, J. M., & Parry, S. J. (1987). Geochemistry of the granitic rocks and their minerals from Serra da Estrela, Central Portugal. *Geochimica et Cosmochimica Acta*, 51(3), 439-454.
- Nicholson, K. (1993). *Geothermal fluids: chemistry and exploration techniques*. Springer-Verlag Berlin Heidelberg New York ISBN 3-540-56017-3, 263p.
- Nishimura, S., & Katsura, I. (1990). Radon in soil gas: Applications in exploration and earthquake prediction. *Geochemistry of Gaseous Elements and Compounds*, 497-533.
- Norton, I. O., & Sclater, J. G. (1979). A model for the evolution of the Indian Ocean and the breakup of Gondwanaland. *Journal of Geophysical Research: Solid Earth (1978–2012)*, 84(B12), 6803-6830.
- Pearson, F. J., & Rightmire, C. T. (1980). Sulphur and oxygen isotopes in aqueous sulphur compounds. *Handbook of environmental isotope geochemistry*, 1, 227-258.
- Petterson, M. G., & Windley, B. F. (1985). Rb Sr dating of the Kohistan arc-batholith in the Trans-Himalaya of north Pakistan, and tectonic implications. *Earth and Planetary Science Letters*, 74(1), 45-57.
- Powell, C. M. (1979). A speculative tectonic history of Pakistan and surroundings: some constraints from the Indian Ocean. In *Geodynamics of Pakistan* 5-24. Geological Survey of Pakistan Quetta.
- Quittmeyer, R. C., Farah, A. B. U. L., & Jacob, K. H. (1979). The seismicity of Pakistan and its relation to surface faults. *Geodynamics of Pakistan*, 271-284.
- Reyes, A. G., Christenson, B. W., & Faure, K. (2010). Sources of solutes and heat in low-enthalpy mineral waters and their relation to tectonic setting, New Zealand. *Journal of Volcanology and Geothermal Research*, 192(3), 117-141.
- Rodríguez, A., Torres, Y., Chavarría, L., & Molina, F. (2008, August). Soil gas radon measurements as a tool to identify permeable zones at las pailas geothermal area, Costa Rica. *Geothermal Training Programme 30th Anniversary workshop*, 26-27.



- Rowley, D. B. (1996). Age of initiation of collision between India and Asia: a review of stratigraphic data. *Earth and Planetary Science Letters*, 145(1), 1-13.
- Sac, M. M., Harmansah, C., Camgoz, B., & Sozibilir, H. (2011). Radon monitoring as the earthquake precursor in fault line in Western Turkey. *Ekoloji*, 20(79), 93-98.
- Savage, D., Bateman, K., Milodowski, A. E., & Hughes, C. R. (1993). An experimental evaluation of the reaction of granite with streamwater, seawater and NaCl solutions at 200 C. *Journal of volcanology and geothermal research*, 57(3), 167-191.
- Searle, M. P., Khan, M. A., Fraser, J. E., Gough, S. J., & Jan, M. Q. (1999). The tectonic evolution of the Kohistan-Karakoram collision belt along the Karakoram Highway transect, north Pakistan. *Tectonics*, 18(6), 929-949.
- Shuja, T. A. (1986). Geothermal areas in Pakistan. *Geothermics*, 15(5), 719-723.
- Shuja, T. A., & Khan, A. L. (1984). Prospects of geothermal energy in Pakistan. *GSP Info Rel.* 242, 22pp.
- Shuja, T. A., & Sheikh, M. I. (1983). A study of geothermal resources of Gilgit and Hunza agencies, northern Pakistan. *Geological Survey of Pakistan Information Release.* 179, 22pp.
- Swakoń, J., Kozak, K., Paszkowski, M., Gradziński, R., Łoskiewicz, J., Mazur, J., & Olko, P. (2004). Radon concentration in soil gas around local disjunctive tectonic zones in the Krakow area. *Journal of environmental radioactivity*, 78(2), 137-149.
- Tanner, A. B. (1964). Radon migration in the ground: A review. *The Natural Radiation Environment. Symposium Proceedings (Chicago, Ill: University of Chicago Press)*. pp. 161-190.
- Thakur, V. C., Jayangondaperumal, R., & Malik, M. A. (2010). Redefining Medlicott–Wadia's main boundary fault from Jhelum to Yamuna: An active fault strand of the main boundary thrust in northwest Himalaya. *Tectonophysics*, 489(1), 29-42.
- Todaka, N., Shuja, T. A., Jamiluddin, S., Khan, N. A., Pasha, M. A., & Iqbal, M. (1999). A preliminary study of geothermal energy resources of Pakistan. *GSP Info Rel.* 407, 93.
- Todaka, N., Shuja, T. A., Jamiluddin, S., Khan, N. A., Pasha, M. A., & Iqbal, M. (1988). A preliminary study for geothermal development project in Pakistan. *Geol Surv Pakistan Mem*, 107, 4-47.
- Tonani, F. B. (1980). Some remarks on the application of geochemical techniques in geothermal exploration. In *Advances in European Geothermal Research*, 428-443. Springer Netherlands.
- Tonarini, S., Villa, I. M., Oberli, F., Meier, M., Spencer, D. A., Pognante, U., & Ramsay, J. G. (1993). Eocene age of eclogite metamorphism in Pakistan Himalaya: implications for India-Eurasia collision. *Terra nova*, 5(1), 13-20.

- Toutain, J. P., & Baubron, J. C. (1999). Gas geochemistry and seismotectonics: a review. *Tectonophysics*, 304(1), 1-27.
- Treloar, P. J., & Izatt, C. N. (1993). Tectonics of the Himalayan collision between the Indian plate and the Afghan block: A synthesis. *Geological Society, London, Special Publications*, 74(1), 69-87.
- Treloar, P. J., Rex, D. C., Guise, P. G., Coward, M. P., Searle, M. P., Windley, B. F., & Luff, I. W. (1989). K-Ar and Ar-Ar geochronology of the Himalayan collision in NW Pakistan: Constraints on the timing of suturing, deformation, metamorphism and uplift. *Tectonics*, 8(4), 881-909.
- Truesdell, A. H. (1976). Geochemical techniques in exploration. In *Proceedings of the 2nd UN Symposium on the Development and Use of Geothermal Resources*. 1, 53-86.
- Truesdell, A. H., & Hulston, J. R. (1980). Isotopic evidence on environments of geothermal systems. In *Handbook of environmental isotope geochemistry*. Fritz, P., & Fontes J.C. eds., 1, 179-226, Elsevier.
- Truesdell, A. H., Nathenson, M., & Rye, R. O. (1977). The effects of subsurface boiling and dilution on the isotopic compositions of Yellowstone thermal waters. *Journal of Geophysical Research*, 82(26), 3694-3704.
- Verchere, A. (1867). On the Geology of Kashmir Himalaya and the Afghan Mountains. *Jour. Asiatic. Soc. Bengal*, 35, 89-133.
- Wadia, D. N. (1928). The geology of Poonch state (Kashmir) and adjacent parts of the Panjab. *Mem. Geol. Surv. India*, 51, 257-268.
- Wadia, D. N. (1931). The syntaxis of the northwest Himalaya: its rocks, tectonics and orogeny. *Rec. Geol. Surv. India*, 65(2), 189-220.
- Wells, N. A., & Gingerich, P. D. (1987). Paleoenvironmental interpretation of Paleogene strata near Kotli, Azad Kashmir, Northeastern Pakistan. *Kashmir Journal of Geology*, 5, 23-41.
- Whitehead, N. E. (1984). Geothermal prospecting by ground radon measurements. *Journal of volcanology and geothermal research*, 20(3), 213-229.
- Yeats, R. S., & Lawrence, R. D. (1982). Tectonics of the Himalayan thrust belt in northern Pakistan. In *US-Pakistan Workshop on Marine Sciences in Pakistan*. (1), 39. Karachi, Pakistan.
- Yeats, R. S., Kausar, A. B., & Nakata, T. (2006). Conferees examine deadly 2005 Kashmir earthquake. *EOS, Transactions American Geophysical Union*, 87(11), 115-115.
- Zaigham, N. A., Nayyar, Z. A., & Hisamuddin, N. (2009). Review of geothermal energy resources in Pakistan. *Renewable and Sustainable Energy Reviews*, 13(1), 223-232.
- Zuhui, L., Yujin, W., Dongrong, C., Youming, L., Aijun, X., & Fuxing, Y. (1993). Prospecting oil and gas deposits with CR-39 detectors. *Nuclear Tracks and Radiation Measurements*, 22(1), 387-392.

APPENDIX-I

Table 1: Radon concentration calculated at sample locations around hot springs along with visible geology at particular point.

Sr. No	Location Code	Geographic Coordinates (Degree, min, sec)		Mean Radon Concentration (kBq m ⁻³)	Lithology
1	A1	33°37'0.58"N	73°56'26.65"E	3.5	Sandstone (Murree Fm)
2	A2	33°37'0.60"N	73°56'34.42"E	4.5	Shale (Eocene-Murree Contact)
3	A3	33°37'0.59"N	73°56'42.19"E	29.5	Shale (Patala Fm)
4	A4	33°37'0.58"N	73°56'49.93"E	7.8	Thick Soil
5	A5	33°37'0.59"N	73°56'57.73"E	10.8	Soil cover
6	A6	33°37'0.62"N	73°57'5.42"E	3.92	Sandstone (Murree Fm)
7	B1	33°36'54.09"N	73°56'26.68"E	3.8	Murree Fm
8	B2	33°36'54.10"N	73°56'34.42"E	5.5	Limestone (Margalla Fm)
9	B3	33°36'54.07"N	73°56'42.16"E	22.8	Soil
10	B4	33°36'54.11"N	73°56'49.92"E	4.87	Soil
11	B5	33°36'54.12"N	73°56'57.67"E	3.29	Loose Gravel (Fluvial)
12	B6	33°36'54.11"N	73°57'5.39"E	4.8	Sandstone (Murree Fm)
13	C1	33°36'47.65"N	73°56'26.64"E	4.29	Fertile Soil
14	C2	33°36'47.64"N	73°56'34.40"E	5.9	Fertile Soil
15	C3	33°36'47.65"N	73°56'42.16"E	9.3	Fertile Soil
16	C4	33°36'47.64"N	73°56'49.96"E	4.7	Limestone (Muzaffarabad Fm)
17	C5	33°36'47.63"N	73°56'57.70"E	2.05	Gravel (River Deposits)
18	C6	33°36'47.62"N	73°57'5.43"E	7.2	Fertile Soil
19	D1	33°36'41.16"N	73°56'26.64"E	2.4	Loose Gravel
20	D2	33°36'41.15"N	73°56'34.39"E	5.02	Loose Gravel
21	D3	33°36'41.14"N	73°56'42.17"E	10.7	Loose Gravel (Bank Deposits)
22	D4	33°36'41.13"N	73°56'49.90"E	3.72	Limestone (Muzaffarabad Fm)
23	D5	33°36'41.14"N	73°56'57.63"E	7.3	Limestone (Muzaffarabad Fm)
24	D6	33°36'41.13"N	73°57'5.41"E	5.8	Soil
25	E1	33°36'34.68"N	73°56'26.65"E	3.1	Regolith (Murree Fm)
26	E2	33°36'34.66"N	73°56'34.39"E	10.2	Fertile Soil
27	E3	33°36'34.67"N	73°56'42.14"E	9.6	Loose Shale (Patala Fm)
28	E4	33°36'34.67"N	73°56'49.93"E	8.23	Loose Shale (Patala Fm)
29	E5	33°36'34.68"N	73°56'57.68"E	5.14	Shale (Patala Fm)
30	E6	33°36'34.69"N	73°57'5.43"E	4.41	Shale (Patala Fm)
31	F1	33°36'28.21"N	73°56'26.65"E	2.7	Young Soil (Murree Fm)
32	F2	33°36'28.17"N	73°56'34.41"E	2.95	Young Soil (Murree Fm)
33	F3	33°36'28.17"N	73°56'42.16"E	23.2	Shale + Soil
34	F4	33°36'28.19"N	73°56'49.93"E	16.9	Stream Deposits
35	F5	33°36'28.20"N	73°56'57.64"E	8.07	Shale (Patala Fm)
36	F6	33°36'28.19"N	73°57'5.43"E	6.32	Shale (Patala Fm)

Table 2: Physical characteristics of water samples from study area along with their geographic coordinates.

Sr. No.	Location Code	Type	Coordinates	Flow Rate (L/s)	Temperature (°C)	pH	EC (µS/cm)	TDS (ppm)
1	Tpp-1	Hot Spring	33°36'43.57"N 73°56'49.35"E	11.8	60.6	6.62	1250	800
2	Tpp-2	Hot Spring	33°36'43.32"N 73°56'49.56"E	4.3	60.5	6.62	1170	790
3	Tpp-3	Hot Spring	33°36'42.90"N 73°56'49.41"E	7.2	59.2	6.62	1190	800
4	Tpp-4	Hot Spring	33°36'43.10"N 73°56'50.16"E	9.1	60.7	6.65	1170	790
5	Tpp-5	Hot Spring	33°36'43.88"N 73°56'49.52"E	15.6	60.8	6.62	1260	810
6	Tps-1	Hot Spring	33°36'37.03"N 73°56'45.50"E	3.6	55.9	6.69	1120	740
8	Tpp-W	Open Well	33°36'46.20"N 73°56'46.61"E	-	18.5	7.44	1020	690
8	Tps-S	Cold Spring	33°36'34.64"N 73°56'46.09"E	5.7	14.1	7.45	510	340
9	Tpp-R	River (North Bank)	33°36'42.75"N 73°56'51.62"E	137516.4	16.8	7.66	230	160
10	Tps-R	River (South Bank)	33°36'39.22"N 73°56'45.65"E	137516.4	14	7.63	230	160

Table 3: Concentration of major cations and anions along with radon concentration in water samples

Sr. No.	Location Code	Type	Ca	Mg	Na	K	HCO ₃	Cl	SO ₄	SiO ₂	Rn ²²²
			ppm						Bq m ⁻³		
1	Tpp-1	Hot Spring	30.93	40.38	153.97	111.42	262	144	14	44.07	8280
2	Tpp-2	Hot Spring	34.45	41.10	133.67	121.76	152	91	22	76.17	7000
3	Tpp-3	Hot Spring	33.74	41.37	129.11	126.32	242	132	26	47.94	7860
4	Tpp-4	Hot Spring	31.30	42.72	151.48	113.14	222	144	24	47.19	8420
5	Tpp-5	Hot Spring	30.57	42.23	149.26	112.47	265	146	26	48.21	9100
6	Tps-1	Hot Spring	35.21	39.12	120.34	118.31	210	122	12	45.23	6970
7	Tpp-W	Open Well	35.98	43.97	42.24	20.33	252	148	32	24.76	6900
8	Tps-S	Cold Spring	38.42	19.81	51.19	36.85	202	28	2	3.518	6320
9	Tpp-R	River (North Bank)	34.78	13.51	20.62	19.65	92	20	6	9.652	5890
10	Tps-R	River (South Bank)	35.16	14.44	28.20	18.90	92	16	9	3.99	5930

Table 4: Calculated reservoir temperatures using different silica geothermometers applied by various authors

Quartz Geothermometers		Calculated Reservoir Temperatures (°C)					
		Tpp-1	Tpp-2	Tpp-3	Tpp-4	Tpp-5	Tps-1
	Surface Temperature	60.6	60.5	59.2	60.7	60.8	55.9
1	Quartz, no steam Fournier, 1977	96.01	122.53	99.86	99.13	100.12	97.19
2	Quartz, no steam Arnorsson et al, 1983	84.36	112.51	88.42	87.65	88.69	85.60
3	Quartz Truesdell, 1976	96.14	122.55	99.97	99.25	100.23	97.32
4	Quartz Giggenbach et al., 1983	70.98	101.63	75.37	74.54	75.66	72.32
5	Quartz, max steam Fournier, 1977	97.54	120.31	100.87	100.24	101.09	98.56
6	Quartz, max steam Arnorsson et al, 1983	96.19	119.18	99.55	98.92	99.78	97.22
7	Chalced Fournier, 1981	65.67	94.34	69.79	69.01	70.06	66.93
8	Chalced Arnorsson et al, 1983	67.34	94.06	71.20	70.47	71.46	68.52
9	Chalced Fournier, 1977	71.65	95.55	75.13	74.47	75.36	72.72
10	Alpha Cris Fournier, 1977	45.74	71.89	49.50	48.79	49.76	46.89
11	Beta Cris Fournier, 1977	-0.63	24.01	2.89	2.22	3.13	0.45
12	Amorphous Fournier, 1977	-18.96	3.93	-15.69	-16.31	-15.47	-17.96
13	Silica Giampaolo et al., 1992	44.57	75.67	48.99	48.15	49.29	45.92

Table 5: Reservoir temperatures calculated using different cation geothermometers applied by various authors

Cation Geothermometers		Calculated Reservoir Temperatures (°C)					
		Tpp-1	Tpp-2	Tpp-3	Tpp-4	Tpp-5	Tps-1
	Surface Temperature	60.6	60.5	59.2	60.7	60.8	55.9
1	Na-K-Ca-Mg (Giggenbach, 1988)	90.96	93.05	93.45	91.14	91.35	92.31
2	K-Ca (Tonani, 1980)	184.01	183.69	180.18	183.56	183.29	186.16
3	K/Mg Giggenbach, 1988	109.22	108.89	112.62	109.92	109.59	112.39
4	Na-K-Ca Beta=1/3	311.64	326.02	332.99	313.83	314.55	329.20
5	Na-K-Ca Beta=4/3	206.44	202.36	206.99	206.57	206.86	196.76
6	Na-K-Ca (Mg corrected)	47.40	49.18	59.88	49.60	48.84	64.54
7	Na/K Truesdell, 1976	585.01	680.57	714.72	596.99	600.40	717.15
8	Na/K Tonani, 1980	686.12	802.97	845.26	700.65	704.80	848.28
9	Na/K Arnorsson et al., 1983	549.97	629.57	657.51	560.07	562.94	659.49
10	Na/K Arnorsson et al., 1983	443.90	485.10	498.87	449.29	450.82	499.83
11	Na/K Fournier, 1979	476.47	525.65	542.25	482.87	484.68	543.42
12	Na/K Nieva&Neiva, 1987	458.31	506.70	523.06	464.60	466.38	524.20
13	Na/K Giggenbach, 1988	462.11	503.15	516.84	467.49	469.01	517.80

Table 6: Results of isotopes analysis; Tritium as TU, Deuterium and oxygen as per mill

Sr. No.	Location Code	Type	Sampling Date	Counting Date	Tritium activity TU (Tritium Units)		$\delta^{18}\text{O}$	$\delta^2\text{H}$
					Measured	On Sampling date		
1	Tpp-1	Hot Spring	27-Feb-15	15-Apr-15	0 \pm 0.2	0 \pm 0.2	-6.27	-39.04
2	Tpp-2	Hot Spring	27-Feb-15	15-Apr-15	0.22 \pm 0.3	0.23 \pm 0.3	-6.41	-39.15
3	Tpp-3	Hot Spring	27-Feb-15	15-Apr-15	0.54 \pm 0.2	0.54 \pm 0.2	-6.39	-39.37
4	Tpp-4	Hot Spring	27-Feb-15	15-Apr-15	0 \pm 0.2	0 \pm 0.2	-6.72	-39.07
5	Tpp-5	Hot Spring	27-Feb-15	15-Apr-15	0 \pm 0.2	0 \pm 0.2	-6.32	-38.86
6	Tps-1	Hot Spring	27-Feb-15	15-Apr-15	0.68 \pm 0.3	0.69 \pm 0.3	-6.15	-36.57
7	Tpp-W	Open Well	27-Feb-15	15-Apr-15	0 \pm 0.3	0 \pm 0.3	-6.77	-37.45
8	Tps-S	Cold Spring	27-Feb-15	15-Apr-15	7.89 \pm 0.5	7.95 \pm 0.5	-5	-21.1
9	Tpp-R	River (North Bank)	27-Feb-15	15-Apr-15	9.75 \pm 0.6	9.82 \pm 0.6	-6.83	-34.42
10	Tps-R	River (South Bank)	27-Feb-15	15-Apr-15	10.28 \pm 0.6	10.36 \pm 0.6	-6.96	-34.46